## Designing a tokamak fusion reactor
## —How does plasma physics fit in?

**Massachusetts Institute of Technology**

# Designing a Tokamak Fusion Reactor – How Does Plasma Physics Fit In?

J.P. Freidberg, F.J. Mangiarotti, and J. Minervini

# Designing a tokamak fusion reactor – how does plasma physics fit in?

**J. P. Freidberg, F. J. Mangiarotti, J. Minervini**

**MIT Plasma Science and Fusion Center**

**Abstract:**

This paper attempts to bridge the gap between tokamak reactor design and plasma physics. The analysis demonstrates that the overall design of a tokamak fusion reactor is determined almost entirely by the constraints imposed by nuclear physics and fusion engineering. Virtually no plasma physics is required to determine the main design parameters of a reactor: $a$, $R_0$, $B_0$, $T_i$, $T_e$, $p$, $n$, $\tau_E$, $I$. The one exception is the value of the toroidal current $I$, which depends upon a combination of engineering and plasma physics. This exception, however, ultimately has a major impact on the feasibility of an attractive tokamak reactor.

The analysis shows that the engineering/nuclear physics design makes **<u>demands</u>** on the plasma physics that must be satisfied in order to generate power. These demands are substituted into the well-known operational constraints arising in tokamak physics: the Troyon limit, Greenwald limit, kink stability limit, and bootstrap fraction limit. Unfortunately, a tokamak reactor designed on the basis of standard engineering and nuclear physics constraints does not scale to a reactor. Too much current is required to achieve the necessary confinement time for ignition. The combination of achievable bootstrap current plus current drive is not sufficient to generate the current demanded by the engineering design. Several possible solutions are discussed in detail involving advances in plasma physics or engineering.

The main contribution of the present work is to demonstrate that the basic reactor design and its plasma physics consequences can be determined simply and analytically.

The analysis thus provides a crisp, compact, logical framework that will hopefully lead to improved physical intuition for connecting plasma physic to tokamak reactor design.

## 1. Introduction

The purpose of this paper is to bridge the gap between fusion reactor design and plasma physics. The main goal is to show how plasma physics directly impacts reactor design. Our target audience is plasma physicists, and not reactor engineers. Indeed, many reactor engineers are already aware of the main results derived here, having deduced them from their own detailed reactor designs [1-8]. Unfortunately, these design results have by and large not permeated into the plasma physics community thereby providing the primary motivation for the present work.

Interestingly and perhaps surprisingly, our analysis demonstrates that the overall design of a standard tokamak fusion reactor is actually dominated by the constraints imposed by nuclear physics and fusion engineering. With one exception, virtually **no input** from achievable plasma physics performance is required to determine the main design parameters of the reactor: $a$, $R_0$, $B_0$, $T_i$, $T_e$, $p$, $n$, $\tau_E$, $I$. The one exception is the value of the toroidal current $I$, which depends upon a combination of engineering and plasma physics. The implication is that a reactor designed on the basis of engineering and nuclear physics constraints, combined with the one exception just noted, makes **demands** on the required zeroth order plasma physics performance that must be satisfied in order to generate power.

It is worth emphasizing this perhaps somewhat surprising result. A reactor based almost entirely on engineering and nuclear physics leads to design values very similar to comprehensive designs which do actually account for all plasma physics constraints. The engineering/nuclear physics design demands certain zeroth order performance from the plasma, without consideration of what is actually achievable.

We note that if currently achievable tokamak plasma performance just happens to meet these demands, the dominant plasma physics component of fusion power would be essentially solved. As might be expected, there are also a substantial number of

additional, less dominant plasma physics constraints that need to be simultaneously satisfied but, for the sake of simplicity these are not considered here. Even so, if the dominant plasma physics could be satisfied this would be a clear signal to the world's fusion program to increase research on engineering and nuclear physics issues.

Unfortunately however, present-day plasma physics performance fails in one crucial area. The reactor-demanded value of $I$ required to achieve a high enough $\tau_E$ for ignited operation is too large. Stated differently, the combination of presently achievable current drive plus bootstrap current in a standard tokamak is too small to sustain the $I$ needed for steady state ignited operation. This is a potential "show stopper" and a solution must be found if the tokamak is going to lead to a power producing reactor.

Several possible solutions are discussed. One class involves advanced plasma physics: increased energy confinement times, higher $\beta$ limits, and increased current drive efficiency. A second class involves advanced engineering: increased maximum allowable magnetic field and demountable superconducting joints. This, in the opinion of the authors has the greatest likelihood of success. A third class relaxes some of the economically driven engineering constraints: larger power output or lower neutron wall loading.

*To summarize, our main conclusion is that the basic as yet unsolved zeroth order plasma physics problem facing the tokamak is the achievement of steady state operation in a high performance, reactor grade plasma. This is a critical goal that the US Fusion Program needs to focus on as fusion research moves forward.*

Before proceeding there is one point worth discussing in order to properly set the stage for the analysis. As stated above, the intended audience for the paper is plasma

physicists. The reason is that the primary contribution of the present work is to show by means of simple, analytical calculations, how one can design a basic tokamak reactor. This has the important advantage of clearly demonstrating how plasma physics enters the reactor design; in other words the analysis provides valuable physical intuition for plasma physicists.

The deliberate simplicity of the analysis obviously makes the numerical accuracy of our results less than that of current state of the art reactor designs [1-8]. Even so, the numerical design parameters derived in our analysis are reasonable and plausible compared to more detailed designs. Still, although the design values are reasonable, our main interest is in illuminating the **reasons** leading to the choice of these parameters.

The strategy of the analysis is to "design" a standard tokamak reactor based on nuclear physics and engineering constraints with only one direct input of plasma physics. Here, "standard" refers to typical values of the engineering constraints used in the design of most US fusion reactors [1-3]. The authors recognize that designs in Europe and Asia sometimes define "standard" differently than in the US [1-3] which can result in more optimistic conclusions. Still, for present purposes we focus on a standard design based on typical US criteria.

Once this design is completed the resulting plasma demands are calculated and then substituted into the well-known zeroth order operational constraints arising in tokamak physics: the Troyon limit, Greenwald density limit, kink stability limit, and maximum bootstrap fraction. The goal is to see whether or not the achievable plasma performance is capable of meeting the required demands. Unfortunately, as already stated, the plasma in a standard tokamak is not very cooperative. Too much current is required to achieve steady state operation thus motivating an investigation into various possible solutions.

Lastly, there is one caveat that needs discussion in order to keep the analysis in perspective. We do not quantitatively account for the critical plasma engineering problem of heat load on the first wall of a fusion reactor in our designs [9]. This is

5

currently an unsolved problem that affects all fusion concepts, not only tokamaks, and is also a potential show stopper in its own right. To support this statement we note that the anticipated heat loads in a reactor are typically almost an order of magnitude larger than in current experiments (and even ITER). This is indeed a very serious problem.

Possible solutions have been suggested including the super-X divertor [10], the snowflake divertor [11], double null divertors [12-14], negative triangularity cross sections [15], and liquid lithium collector plates [16]. However, there has not as yet been a successful experimental demonstration at high heat loads of any of these technologies. This is a task for the near future. Consequently, it is not possible at present to reliably quantify how the heat load problem directly enters the design of a reactor. Instead, we define a figure of merit which measures how difficult it will be to satisfy the heat load requirement. This figure of merit makes it possible to compare different design strategies but in all cases it must be assumed that a satisfactory solution can be found.

## 2. Formulation of the design problem

### 2.1 The design goals:

The aim of the design is to calculate the basic parameters of a tokamak fusion reactor as determined by the critical engineering and nuclear physics constraints plus the one-exception plasma physics needed to determine $I$. The reactor model is illustrated in Fig. 1. The dominant components of the reactor are the plasma, blanket region (first wall, blanket, shield, and vacuum chamber), and toroidal field magnets. The analysis has also been carried out including the central solenoid, but the overall results are very similar and for the sake of simplicity this coil is ignored

The parameters to be determined from the analysis are as follows:

| Quantity | Symbol |
|---|:---:|
| Minor radius of the plasma | $a$ |
| Major radius of the plasma | $R_0$ |
| Elongation | $\kappa$ |
| Thickness of the blanket region | $b$ |
| Thickness of the TF magnets | $c$ |
| Plasma temperature | $T$ |
| Plasma density | $n$ |
| Plasma pressure | $p$ |
| Energy confinement time | $\tau_E$ |
| Magnetic field at $R = R_0$ | $B_0$ |
| Normalized plasma pressure | $\beta$ |
| Plasma current | $I$ |
| Normalized inverse current | $q_*$ |
| Bootstrap fraction | $f_B$ |

Table 1. Reactor parameters to be determined.

The analysis presented in the paper yields reasonable values for all of these parameters, comparable to far more sophisticated designs [1-8]. Even more important, the analysis gives a <u>reason</u> for determining all of these values. It is worth re-emphasizing that the final design <u>demands</u> certain values for the plasma temperature, pressure, density, and current for a successful fusion reactor. These are not free parameters to be determined by the best efforts of plasma physicists.

**2.2 Engineering and nuclear physics constraints:**

There are a number of basic engineering and nuclear physics constraints that directly enter into the design of a "standard" tokamak reactor. The nuclear physics constraints, involving cross sections, are straightforward but the engineering constraints warrant some discussion. The values for the main engineering constraints are typical of those used in most fusion reactor designs [1-8]. Specifically, the electric power output is set to $P_E = 1000 \ MW$ to maximize economy of scale benefits without overstressing grid capacity and/or deterring investor interest.

Another critical constraint is the maximum allowable neutron wall loading. Many designs typically assume $P_W \approx 4 \ MW \ / \ m^2$. We recognize that some designs [17] use lower values, on the order of $P_W \approx 1 - 2 \ MW \ / \ m^2$, which in general leads to a larger, easier to build, but more expensive plant. However, even at this early stage of fusion reactor development many US designs often place a strong emphasis on perceived economics. In fact, D. Whyte has presented a calculation [18] that shows when blanket/first wall replacement time and cost are taken into account economic breakeven is not possible unless a neutron wall loading of at least $P_W = 3 - 5 \ MW \ / \ m^2$ is achievable. This crucial economic issue plays a major role in US designs, and further motivation by D. Whyte's recent analysis leads us to choose an admittedly aggressive value of $P_W = 4 \ MW \ / \ m^2$ for our standard reference reactor.

Similarly, most reactor designs place a strong demand on steady state operation [1-8]. In contrast, some designs [17, 19] consider the possibility of a pulsed reactor, an acknowledgement of the difficulty of achieving steady state operation. While pulsed operation alleviates the problems of achieving steady state, it introduces new engineering problems associated with cyclical thermal and mechanical stresses. In the US steady state is currently considered to be the lesser of two evils and this is the choice made here.

A related constraint involving the overall power balance is the maximum allowable recirculating power fraction. Typically, an economically viable power plant recirculates

10% or less of its total electric power output. To ease this difficult constraint for fusion we allow a maximum recirculating fraction of 15% of which 10% corresponds to the current drive power needed for steady state operation.

Next, consider the magnets. The maximum allowable magnetic field, which occurs on the inboard midplane of the TF coil, is taken as $B_{max} = 13 \; T$, a realistic value for current state of the art Niobium-Tin superconducting TF magnets [4, 20]. Below this field the magnet should not quench. In terms of design there are two additional magnet engineering requirements: (1) the maximum allowable mechanical stress on the supporting structural material is $\sigma_{max} = 600 \; MPa$ and (2) the maximum allowable current density averaged over the whole winding pack (i.e. superconducting cables plus mounting structure) is $J_{max} = 20 \; MA/m^2$. The superconducting cables themselves carry a current density of $J_{SC} = 45 \; MA/m^2$ but it is the full winding pack that contributes to the size of the coil thickness $c$. These are typical values for large scale Niobium-Tin SC magnets and are very similar to the values for ITER [20].

The final quantity that needs discussion is the value of magnetic field in the center of the plasma. Specifically, a fundamental quantity that defines a tokamak is the magnetic field $B = B_0$ at $R = R_0$. Here there is a basic conflict between engineering and plasma physics. Engineering obviously would like $B_0 = 0$ to minimize the cost. On the other hand, plasma physics would like $B_0 = \infty$ to maximize performance.

The strategy adopted here assumes that $B_0$ is a given fixed parameter but whose value is initially unspecified. In principle, we could design a sequence of reactors as a function of $B_0$. The choice for $B_0$ would then be the minimum value that satisfies all the plasma physics constraints. It is important though to make sure that the resulting $B_0$ does not lead to a field on the inboard side of the coil that exceeds the maximum allowable limit, which has been set to $B_{max} = 13 \; T$. It turns out that the value of $B_0$ for good plasma physics always exceeds the $B_{max} = 13 \; T$ limit. The practical

implication is that the value of $B_0$ is set in any given design until the condition $B_{max} = 13\ T$ is reached.

Note that the constraint values described above, while typical, can vary somewhat from design to design. However, these variations are not critical to the basic design analysis. For convenience the engineering constraints plus the self-explanatory nuclear physics constraints are summarized in Table 2.

| Quantity | Symbol | Limiting Value |
|---|---|---|
| Electric power output | $P_E$ | 1000 $MW$ |
| Maximum neutron wall loading | $P_W$ | 4 $MW\,/\,m^2$ |
| Maximum magnetic field at the coil | $B_{max}$ | 13 $T$ |
| Maximum mechanical stress on the magnet: | $\sigma_{max}$ | 600 $MPa$ |
| Maximum superconducting coil current density averaged over the winding pack | $J_{max}$ | 20 $MA\,/\,m^2$ |
| Thermal conversion efficiency | $\eta_T$ | 0.4 |
| Maximum RF recirculating power fraction | $f_{RP}$ | 0.1 |
| Wall to absorbed RF power conversion efficiency | $\eta_{RF}$ | 0.4 |
| Temperature at $\left[\left\langle \sigma v \right\rangle / T^2\right]_{max}$ | $\overline{T}$ | 14 $keV$ |
| Fast neutron slowing down cross section in $Li$-7 | $\sigma_S$ | 2 $barns$ |
| Slow neutron breeding cross section in $Li$-6 | $\sigma_B$ | 950 $barns$ at 0.025 $eV$ |

Table 2. Basic engineering and nuclear physics constraints

Overall, it is fair to say that the constraints listed in Table 2 almost completely determine the reactor design and make no reference to plasma physics. As the analysis progresses we shall see that plasma physics actually enters the design in two ways.

First, the empirical energy confinement time will be directly used to calculate the current required for steady state operation. Second and indirectly, the need to achieve good plasma performance drives the design to high values of $B_0$. When these plasma requirements are quantified, we shall see that achievable plasma performance is not very cooperative when it comes to reactor design.

Lastly, it is interesting for a moment to consider a somewhat different mission – a steady state pilot plan rather than a full scale power reactor. In this case, as shown by the ARC design [21], a combination of aggressive plasma physics, magnet engineering, and blanket design leads to a compact, high field device producing an output power of only $283\ MW$. Although the ARC recirculating power fraction is about $f_{RP} = 0.3$, it operates at a lower wall loading $P_W = 2.5\ MW\,/\,m^2$, and its absolute cost should be much smaller because of its lower power out. This last feature is a major advantage in minimizing the cost of fusion development. The present analysis with a noticeably different set of constraints could in principle be used to analyze pilot plant design. However, this analysis is deferred until the future.

**2.3 Design strategy**

Returning again to the full scale reactor we now determine the various quantities entering the design one by one. The basic strategy of the analysis is to express each design requirement in terms of the plasma minor radius $a$. After all the engineering and nuclear physics constraints have been taken into account, the resulting plasma demands are then compared to the achievable plasma performance as determined by years of experimental experience. This comparison is carried out as a function of $a$ to see which if any values might lead to an attractive reactor.

As the analysis progresses typical values for each of the reactor parameters are estimated by choosing $a$ such that $R_0\,/\,a = 4$, a standard value for a tokamak reactor.

There is no justification for choosing $a$ this way – this is simply done to give readers a convenient reference design to keep in mind. The actual dependence of the reactor parameters on $a$ is examined once all the requirements have been taken into account.

## 3 Geometric requirements

### 3.1 The plasma elongation $\kappa$

The first step in the reactor design is determining the ellipticity $\kappa$. This is a non-controversial choice which is made at the beginning of the analysis in order to simplify various geometric expressions that appear later in the analysis. The choice is non-controversial because the impact of larger ellipticity is favorable for both engineering and plasma physics. Ellipticity reduces the cost and improves plasma performance.

However, both plasma physics and engineering also place limits on the maximum achievable ellipticity in practical designs. The plasma physics limitations result from the onset of vertical instabilities when $\kappa$ becomes too large [22]. Engineering enters the picture through feedback, which can stabilize these instabilities within certain engineering limits related to the practical design of control systems. That is, the growth rates of the instabilities, proportional to $\kappa$, must be sufficiently low that practically achievable control systems can be designed with an adequately fast response time.

In the analysis that follows we choose

$$\kappa = 1.7 \tag{1}$$

a value that has been readily achieved in existing experiments, is anticipated for ITER, and is typical in many sophisticated reactor designs. We recognize that this value may decrease somewhat as the aspect ratio increases but there is no simple, universally

agreed upon, engineering based functional relation of the form $\kappa \leq \kappa_{\max}(\varepsilon)$ presently available. For simplicity we just set $\kappa = 1.7$ for all designs in our analysis.

**3.2 The blanket region thickness $b$ :**

The "blanket" region consists of the first wall, blanket-and-shield, and vacuum chamber. Each of these components is assumed to be a toroidally homogeneous, monolithic structure. A simple planar model of the region is illustrated in Fig. 2. The largest of these components is the blanket which is the main focus of the analysis in this section. The blanket consists of the following sub-regions: (1) a narrow region for neutron multiplication, (2) a moderating region to slow down fast fusion neutrons, (3) a breeding region to produce tritium.

There are many options for the overall blanket design [23, 24]. One can use solid or liquid breeding materials; pure lithium or compounds containing lithium; water, helium, or liquid salts as a coolant; a variety of structural materials; a vacuum chamber location which can be either inside or outside of the blanket. In spite of this wide range of options there are several universal nuclear properties that set the geometric size of the blanket, which is about the same for all options. In fact it is not unreasonable to say that the entire scale of a fusion reactor is largely determined by the slowing down mean free path of 14.1 $MeV$ neutrons in lithium. This point is demonstrated as the analysis progresses.

The calculation below presents a simple model for determining the width of the combined slowing down and breeding sub-regions. These are the dominant contributions to the blanket size which is only slightly less than the overall width $b$. We begin by noting that the breeding cross section in Li-6 is very large, on the order of 1000 $barns$, for thermal neutrons. It is negligible for 14.1 $MeV$ neutrons. Thus it is important to slow the 14.1 $MeV$ fusion neutrons down to near thermal energies in order

to achieve effective breeding. Most of the energy conversion from fusion neutrons to steam takes place in the slowing down region.

For purposes of calculation, assume the blanket is composed of pure natural lithium. A beam of 14.1 $MeV$ fusion neutrons impinges from the left. Slowing down is dominated by collisions of high energy neutrons with Li-7 nuclei, the dominant component of natural lithium. The basic slowing down physics is determined by the energy balance relation for neutrons.

Once the neutrons have slowed downed they enter the breeding region. Breeding requires Li-6 which has a 0.075 fractional concentration of natural lithium. The basic breeding physics involves the mass balance relation for neutrons. Each time a slow neutron has a nuclear collision with an Li-6 nucleus, the neutron is lost and a tritium nucleus is born.

The governing equations for slowing down and breeding can be written as

$$\frac{dE}{dx} = -\frac{E}{\lambda_S} \qquad E(0) = 14.1 \ MeV \qquad \text{Energy balance}$$
$$\frac{d\Gamma}{dx} = -\frac{\Gamma}{\lambda_{BR}} \qquad \Gamma(0) = \Gamma_0 \qquad \text{Mass balance}$$

$$(2)$$

Here $E = mv^2 / 2$ is the neutron energy and $\lambda_S = 1 / N_7 \sigma_S$ is the mean free path for slowing down. The quantity $N_7 = 4.6 \times 10^{28} \ m^{-3}$ is the number density of Li-7 and $\sigma_S$ is the slowing down cross section. Since slowing down collisions are basically hard sphere collisions a reasonable approximation is that $\sigma_S \approx 2 \ barns = $ constant [25]. This corresponds to $\lambda_S = 0.1 \ m$.

In the mass balance equation $\Gamma(x) = nv$ is the neutron flux, $\Gamma_0$ is the input flux, $\lambda_{BR}(x) = 1 / N_6 \sigma_{BR}$ is the mean free path for breeding and $N_6 = 0.075 N_7 = 0.34 \times 10^{28} \ m^{-3}$ is the number density of Li-6. For slow neutrons the breeding cross section can be reasonably well approximated by the following energy

14

dependent relation $\sigma_{BR}(x) = \sigma_B \left(E_T / E\right)^{1/2}$ where $\sigma_B = 960 \, barns$ and $E_T = 0.025 \, eV$ [25]. Observe the large nuclear cross section for breeding at thermal energies.

Equation (2) can be easily solved for $E(x)$ and $\Gamma(x)$. The solution for $\Gamma(x)$ can then be inverted to determine $\Delta x$, the blanket thickness required to reduce the input neutron flux to a sufficiently low level $\Gamma_b$ corresponding to essentially complete breeding of the fusion neutrons. We shall assume that $\Gamma_b / \Gamma_0 = 10^{-5}$. The desired expression for $\Delta x$ is found to be

$$\Delta x = \lambda_S \ln\left(1 + \alpha_B \ln\frac{\Gamma_0}{\Gamma_b}\right) = 0.9 \, m \tag{3}$$

where $\alpha_B = (\lambda_B / \lambda_S)\left(E_F / E_T\right)^{1/2} = 710$ and $\lambda_B = 1 / N_6 \sigma_B = 0.003 \, m$. The solution is not very sensitive to the value of $\Gamma_b / \Gamma_0$ since it appears in a double logarithm.

The blanket is about 1 meter thick. The full dimension $b$ entering the analysis requires that we add to $\Delta x$ the first wall thickness, the neutron multiplication region, the shield, and the vacuum chamber. Comparisons with much more sophisticated blanket studies [5, 26] using more realistic combinations of materials in the blanket plus a higher degree of optimization, suggest that a reasonable, perhaps slightly optimistic, value for the full dimension is approximately

$$b \approx 1.2 \, m \tag{4}$$

and this is the value used in the analysis that follows.

The parameter $b$ has now been determined solely by nuclear physics constraints. There is not much that can be done to reduce this value and its value essentially sets the geometric scale for the whole reactor.

**3.3 The wall loading limit $R_0 = R_0(a)$:**


As stated, the goal of the mathematical analysis is to express all quantities of interest as a function only of $a$ and $b$. Since $b$ is known this ultimately leads to a one parameter family of constraint requirements. Keeping this strategy in mind the next step is to determine a relationship between $R_0$ and $a$ from the neutron wall loading constraint.

The relationship is straightforward to derive. We simply equate the total neutron power resulting from fusion reactions to the maximum allowable neutron power passing through the first wall: $P_n = P_W S$. Here $P_n (MW)$ is the total neutron power, $P_W (MW / m^2)$ is the neutron wall loading limit, and $S \approx 4\pi^2 R_0 a [(1 + \kappa^2) / 2]^{1/2}$ is the approximate surface area of the plasma.

The neutron power can easily be related to the electric power output of the reactor by recalling that $P_n = (E_n / E_F) P_F$ with $E_n = 14.1 \ MeV$, $E_F = 22.4 \ MeV$, and $P_F$ = the total thermal power output from neutron and alpha fusion reactions plus Li-6 breeding reactions. The thermal power is converted into electrical power output by means of a steam cycle with a thermal efficiency $\eta_T = 0.4$: $P_F = P_E / \eta_T$

Combining these results leads to the desired relationship between $R_0$ and $a$,


$$R_0 = \left[ \frac{1}{4\pi^2} \frac{E_n}{E_F} \frac{P_E}{\eta_T P_W} \left( \frac{2}{1 + \kappa^2} \right)^{1/2} \right] \left( \frac{1}{a} \right) = \frac{7.16}{a} \ m \qquad (5)$$


The major radius scales inversely with $a$ but is independent of $B_0$. For the reference case which assumes that $R_0 / a = 4$, we see that Eq. (5) implies that $a = 1.34 \ m$ and $R_0 = 5.34 \ m$.

**3.4 The central magnetic field** $B_0 = B_0(a,b)$

The toroidal magnetic field at the center of the plasma can be accurately approximated from the well-known relation $B_\phi(R) = B_0(R_0 \,/\, R)$. Since the magnetic field at the inboard side of the TF coil is set by the maximum allowable value of $B_{max}$ it follows that

$$B_0 = B_{max}\left[1 - \frac{a+b}{R_0}\right] = B_{max}\left[1 - 0.14\,a\,(a+b)\right] = 6.8 \text{ T} \tag{6}$$

The central field is about one-half of the maximum field.

**3.5 The coil thickness** $c = c(a, B_0)$ **:**

The toroidal field (TF) magnets are a major component of the reactor and some care is needed to obtain simple but reliable values for the coil thickness. Each TF coil is assume to be a flat pancake magnet. The coils are in wedging contact with each other at the inboard side and there are obviously spaces separating the coils at the outboard side. We do, however, neglect TF ripple effects..

Our model assumes that the total coil thickness $c$ is comprised of two contributions,

$$c = c_M + c_J \tag{7}$$

Here, $c_M$ represents the thickness of structural material needed to mechanically support the magnet stresses while $c_J$ represents the thickness of the superconducting winding pack (i.e. superconducting cable plus mounting structure) required to carry the TF coil current.

17

Consider first the evaluation of $c_M$. There are several forces that contribute to the TF magnet stress including the tensile force, the centering force, and the out of plane bending force. The largest contributions arise from the centering force and tensile force and thus for simplicity, the bending force is hereafter neglected. The strategy is to separately calculate the stresses due to the tensile force plus the centering force and combine them to form the Tresca stress which is then set equal to the maximum allowable stress. Use of the Tresca stress is made for convenience since it leads to a simple analytic expression for $c_M$. Keep in mind that the maximum allowable material stress for high strength cryogenic structural materials is on the order of $600\ MPa$ [27]. This value is not conservative but should be achievable, even with presently availability high strength alloys.

The quantity $c_M$ is now calculated as follows. To begin, consider the effect of the tensile force. We split the TF magnet into an upper and lower half as shown in Fig. 3a and calculate the upward force on the top half of the magnet due to the magnetic field. Interestingly, as is well known [28], this force is independent of the magnet shape and only depends on the mid-plane dimensions of the coil. The upward force, expressed in terms of $B_0$ is given by

$$F_Z = \frac{\pi}{\mu_0} B_0^2 R_0^2 \ln\left(\frac{1 + \varepsilon_B}{1 - \varepsilon_B}\right) \tag{8}$$

where $\varepsilon_B = (a + b) / R_0$.

Next, note that the upward force $F_Z$ is balanced by two equal tensile forces $F_T$ at each end of the upper half of the TF magnet. In other words $F_Z = 2F_T$. Equality of the forces is assumed for mathematical simplicity. In actual detailed designs the inner leg force is slightly higher than the outer leg force but this effect is neglected here. We

further assume that the TF coil is designed to have approximately constant tension around its perimeter so that $c_M =$ constant around the magnet.

Using the assumption that neighboring coils are in wedging contact with each other on the inboard side it is then easy to calculate the total tensile force produced by the $N$ magnets. We find

$$F_T = \sigma_T A_T = \pi \sigma_T \left[ (R_0 - a - b)^2 - (R_0 - a - b - c_M)^2 \right] \tag{9}$$

where $\sigma_T$ is the portion of the maximum stress $\sigma_{max}$ balancing the tensile forces.

Both terms in the tensile stress force balance relation have now been calculated. After setting $F_Z = 2F_T$ we solve for $\sigma_T$ obtaining

$$\sigma_T = \frac{B_0^2}{2\mu_0} \frac{\ln[(1 + \varepsilon_B) / (1 - \varepsilon_B)]}{\varepsilon_M (2 - 2\varepsilon_B - \varepsilon_M)} \tag{10}$$

Here, $\varepsilon_M = c_M / R_0$.

A similar calculation holds for the centering force. The rectangular model for the magnet shape leads to a simple expression for the inboard and outboard radial forces over a narrow toroidal wedge of coil of angular extent $\Delta\phi$ as shown in Fig. 3b.

$$F_{in} = \frac{2B_0^2}{\mu_0} \frac{(\kappa a + b)R_0 \Delta\phi}{2 - 2\varepsilon_B - \varepsilon_M}$$
$$\tag{11}$$
$$F_{out} = \frac{2B_0^2}{\mu_0} \frac{(\kappa a + b)R_0 \Delta\phi}{2 + 2\varepsilon_B + \varepsilon_M}$$

The net inward force is just $F_R = F_{in} - F_{out}$.

The force $F_R$ is balanced by the compression stress due to wedging on the inboard side of the magnet. Referring again to Fig. 3b we see that $F_C$ is given by

$$F_C = \sigma_C A_C = 2\sigma_C c_M (\kappa a + b) \tag{12}$$

where $\sigma_C$ is the portion of the maximum stress $\sigma_{max}$ balancing the centering force. Equilibrium force balance requires that $F_R = 2F_C \sin(\Delta\phi / 2) \approx F_C \Delta\phi$ which leads to an expression for $\sigma_C$ that can be written as

$$\sigma_C = \frac{B_0^2}{\mu_0}\frac{1}{\varepsilon_M}\left(\frac{2}{2 - 2\varepsilon_B - \varepsilon_M}\right)\left(\frac{2\varepsilon_B + \varepsilon_M}{2 + 2\varepsilon_B + \varepsilon_M}\right) \approx \frac{B_0^2}{\mu_0}\frac{1}{\varepsilon_M}\left(\frac{2}{2 - 2\varepsilon_B - \varepsilon_M}\right)\left(\frac{\varepsilon_B}{1 + \varepsilon_B}\right) \tag{13}$$

For mathematical simplicity, the second form neglects $\varepsilon_M$ in the second parenthesis, a good approximation since $\varepsilon_M$ is usually substantially smaller then $2\varepsilon_B$.

The quantity $\varepsilon_M$ is now determined by setting the Tresca stress, $\sigma_T + \sigma_C$, equal to its maximum allowable value, $\sigma_{max}$; that is $\sigma_T + \sigma_C = \sigma_{max}$. The result is a quadratic algebraic equation for $\varepsilon_M$. A straightforward calculation yields an expression for $c_M = \varepsilon_M R_0$,

$$c_M = R_0 \left\{ 1 - \varepsilon_B - \left[ (1 - \varepsilon_B)^2 - \alpha_M \right]^{1/2} \right\}$$

$$\alpha_M = \frac{B_0^2}{\mu_0 \sigma_{max}}\left[ \frac{2\varepsilon_B}{1 + \varepsilon_B} + \frac{1}{2}\ln\left(\frac{1 + \varepsilon_B}{1 - \varepsilon_B}\right)\right] \tag{14}$$

For the reference case $c_M = 0.39\ m$.

The final quantity to be calculated is $c_J$, the thickness of superconducting winding pack required to carry the current. This quantity is also most easily calculated at the inside of the magnet where the field is maximum. Since adjacent coils are in contact with one another this provide a total current carrying area equal to $A$ as defined in Eq. (9). The current $I$ passing through this area can be expressed in terms of

$J_{max} \approx 20$ MA/m$^2$, the maximum allowable overall current density for the superconducting coils [1,20]: $I = J_{max}A$. At the inside of the coil, $I$ produces a toroidal magnetic field $B_{max} = \mu_0 I / 2\pi(R_0 - a - b)$. We now make use of the fact that $B_{max} = B_0 / (1 - \varepsilon_B)$. Simple elimination then yields an expression for $c_J$ in terms of the geometry and $B_0$,

$$c_J = R_0 \left\{ 1 - \varepsilon_B - \left[ (1 - \varepsilon_B)^2 - \alpha_J \right]^{1/2} \right\}$$

$$\alpha_J = \frac{2B_0}{\mu_0 R_0 J_{max}}$$

(15)

For the reference case $c_J = 0.575 \; m$.

Based on this discussion the value of the total TF magnet thickness is written as

$$c = R_0 \left\{ 2(1 - \varepsilon_B) - \left[ (1 - \varepsilon_B)^2 - \alpha_M \right]^{1/2} - \left[ (1 - \varepsilon_B)^2 - \alpha_J \right]^{1/2} \right\}$$

(16)

The total reference value for the magnet thickness is $c = 0.965 \; m$

In terms of the geometry, at this point in the analysis the ellipticity $\kappa$ and blanket region thickness $b$ have been determined. In addition, the major radius $R_0$ and TF coil thickness $c$ have been expressed as a function of $a$. These relations do not depend on plasma physics, only the engineering and nuclear physics constraints previously discussed. The next task is to see how these constraints place demands on the plasma physics performance.

## 4. Plasma physics requirements

By combining the geometric relations above with the remaining engineering constraints it is straightforward to calculate the <u>required</u> plasma temperature, pressure, density, and energy confinement time as well as the plasma $\beta$, all as a function of $a$. With the addition of some plasma physics it is also possible to calculate the plasma current, the kink safety factor, and the bootstrap fraction. There is additional plasma physics involving ELMs, profile effects, energetic particle effects, etc. We view these effects as important but not dominant in terms of reactor design and thus, for the sake of simplicity, they are not explicitly considered in our analysis which proceeds as follows.

**4.1 The average plasma temperature $\bar{T}$**

We assume that the plasma operates at a sufficiently high density so that $T_e = T_i \equiv T$. Thus, the fusion power density produced in the plasma is given by

$$S_P = \frac{1}{16}(E_n + E_\alpha)p^2 \frac{\langle \sigma v \rangle}{T^2} \quad W / m^3 \tag{17}$$

where $p = 2nT$. As usual we maximize $S_P$ by maximizing the ratio of $\langle \sigma v \rangle / T^2$. This maximum occurs at $T \approx 14 \, keV$. It actually has a relatively flat maximum at these temperatures so one can change this value somewhat without much penalty. In any event, for present purposes we choose

$$\bar{T} = 14 \, keV \tag{18}$$

where $\bar{T}$ is the volume averaged temperature.

## 4.2 The average plasma pressure $\overline{p}$

The plasma pressure is determined by the requirement that the total thermal power generated by fusion reactions in the specified reactor geometry produces the required electrical output power. All the fusion power, including the $4.8\ MeV$ per breeding reaction with Li-6, is converted into steam which is then transformed into electricity with a thermal efficiency $\eta_T = 0.4$. Thus, power balance (with $E_F = 22.4\ MeV$) requires

$$\frac{\eta_T E_F}{16} \int p^2 \frac{\langle \sigma v \rangle}{T^2} d\mathbf{r} = P_E \tag{19}$$

To evaluate the integral, plasma profiles must be specified. We make the important assumption that that the profiles have simple, standard forms. No large internal or edge transport barriers are allowed in this part of the analysis. The profiles are given by

$$T = \overline{T}(1+\nu_T)(1-\rho^2)^{\nu_T} = 2\overline{T}(1-\rho^2)$$
$$p = \overline{p}(1+\nu_p)(1-\rho^2)^{\nu_p} = 2.5\overline{p}(1-\rho^2)^{3/2} \tag{20}$$
$$n = \overline{n}(1+\nu_n)(1-\rho^2)^{\nu_n} = 1.5\overline{n}(1-\rho^2)^{1/2}$$

Here, $R = R_0 + a\rho\cos\theta$, $Z = \kappa a\rho\sin\theta$, and an over-bar denotes average value. The plasma lies in the region $0 \leq \rho \leq 1$. Note that the relation $p = 2nT$ implies that $\overline{p} = 2[(1+\nu_T)(1+\nu_n)/(1+\nu_p)]\overline{n}\overline{T} = 2.4\overline{n}\overline{T}$ and $\nu_p = \nu_T + \nu_n$. The quantities $\nu_T, \nu_p, \nu_n$ are free parameters which for standard profiles have been chosen as $\nu_T = 1, \nu_p = 3/2$, and $\nu_n = 1/2$. Lastly, we use the simple analytic approximation for $\langle \sigma v \rangle$ given by

$$\langle \sigma v \rangle = \exp\left[k_0 + k_1(\ln T) + k_2(\ln T)^2 + k_3(\ln T)^3 + k_4(\ln T)^4\right] \qquad (21)$$

where $k_0 = -60.4593$, $k_1 = 6.1371$, $k_2 = -0.8609$, $k_3 = 0.0356$, and $k_4 = -0.0045$. These assumptions are substituted into Eq. (19) leading to an expression for the required average pressure,

$$\overline{p} = \left[\frac{4}{\pi^2}\left(\frac{1+\nu_T}{1+\nu_p}\right)^2 \left(\frac{P_E}{\eta_T E_F R_0 a^2 \kappa}\right)\frac{\overline{T}^2}{\int_0^1 (1-\rho^2)^{2\nu_n}\langle \sigma v \rangle \rho\, d\rho}\right]^{1/2} \qquad (22)$$

All the quantities on the right hand side are either known or expressible in terms of $a$. After a straightforward numerical evaluation of the integral we obtain

$$\overline{p} = \frac{8.76}{a^{1/2}} \ atm \qquad (23)$$

Observe that the pressure scales as $a^{-1/2}$ but is independent of $B_0$. For the reference case $\overline{p} = 7.57 \ atm$. In terms of plasma physics parameters the required beta corresponds to

$$\beta = \frac{2\mu_0 \overline{p}}{B_0^2} = \frac{1.31}{a^{1/2}(1-\varepsilon_B)^2} \ \% \qquad (24)$$

and has the value $\beta = 4.13\,\%$.

**4.3 The average plasma density $\overline{n}$**

The average plasma density is easily obtained from the relation $p = 2nT$ and is given by

$$\overline{n} = \left[ \frac{1 + \nu_p}{2(1 + \nu_T)(1 + \nu_n)} \right] \frac{\overline{p}}{\overline{T}} = \frac{1.66}{a^{1/2}} \quad (10^{20} m^{-3}) \tag{25}$$

The reference value is $\overline{n} = 1.43 \times 10^{20} \ m^{-3}$.

**4.4 Energy confinement time $\tau_E$**

The energy confinement time is determined by the requirement that in steady state the thermal conduction losses are balanced by alpha particle heating. The plasma is assumed to be ignited. This power balance can be written as

$$P_\alpha = \frac{3}{2\tau_E} \int p \, d\mathbf{r} = \frac{3}{2} \frac{V_P \overline{p}}{\tau_E} \tag{26}$$

where $P_\alpha = (E_\alpha / E_F)(P_E / \eta_T)$ and $V_P = 2\pi^2 R_0 a^2 \kappa$. Solving for $\tau_E$ leads to

$$\tau_E = 3\pi^2 R_0 a^2 \kappa \left( \frac{E_F}{E_\alpha} \frac{\eta_T}{P_E} \right) \overline{p} = 0.81 a^{1/2} \quad \text{sec} \tag{27}$$

The required energy confinement time scales as $a^{1/2}$ and is also independent of $B_0$. For the reference case $\tau_E = 0.94$ sec.

**4.5 The plasma current $I$**

All of the required plasma parameters have so far required no direct input from plasma physics. If we now combine an important plasma physics constraint with the engineering requirement on $\tau_E$ we can derive an expression for the current $I$ in terms of $a$, in addition to a subsidiary relation for the bootstrap fraction $f_B$. This is where the plasma physics enters the reactor design.

The plasma current is determined by equating the required energy confinement time to the empirically determined energy confinement time. For ELMy H-modes the empirical $\tau_E$ is given by [29]

$$\tau_E = 0.145 H \frac{I^{0.93} R^{1.39} a^{0.58} \kappa^{0.78} \bar{n}^{-0.41} B_0^{0.15} A^{0.19}}{P_\alpha^{0.69}} \quad \sec \tag{28}$$

Here, all quantities have been previously defined except $A = 2.5$ which is the average atomic mass and the H-mode enhancement factor $H$ which for now is set to unity: $H = 1$. Also the units are $I(MA)$, $\bar{n}(10^{20}\, m^{-3})$, and $P_\alpha(MW)$. We substitute $P_\alpha$ from Eq. (26) and solve for $I$. The result is

$$I = \frac{7.98}{H^{1.08}} \frac{\tau_E^{1.08}}{R_0^{1.49} a^{0.62} \kappa^{0.84} \bar{n}^{-0.44} B_0^{0.16} A^{0.20}} \left[ \left( \frac{E_\alpha}{E_F} \right) \frac{P_E}{\eta_T} \right]^{0.74} = 12.1 \frac{a^{1.63}}{B_0^{0.16}} \quad MA \tag{29}$$

The required current scales approximately as $a^{5/3}$ and is nearly independent of $B_0$. For the reference case $I = 14.3\, MA$. In terms of the kink safety factor the current is equivalent to

$$q_* = \frac{2\pi a^2 B_0}{\mu_0 R_0 I} \left( \frac{1+\kappa^2}{2} \right) = 0.112\, a^{1.37} B_0^{1.16} \tag{30}$$

with a reference value $q_* = 1.56$.

## 4.6 The bootstrap fraction $f_B$

The required bootstrap fraction follows from a simple analysis of current drive efficiency and the constraint that the RF recirculating power be (less than) 10% of the electrical power out: $f_{RP} = P_{RF} / P_E = 0.1$. Since current drive efficiency, even at its highest, is still relatively low, this is the dominant contribution to the recirculating power. For our reactor the current is driven by lower hybrid waves, launched from the outside, which have the highest efficiency as compared to other driving mechanisms.

Since $P_E = 1000 \ MW$ we see that $P_{RF} = 100 \ MW$ is available to drive current. Of this $100 \ MW$ we assume that there is a 50% conversion efficiency from wall power to klystron power and that 80% of the total klystron power is absorbed in the plasma for driving current. Therefore, the power that actually drives the current is equal to

$P_{CD} = \eta_{RF} P_{RF} = \eta_{RF} f_{RP} P_E = (0.5)(0.8)(0.1) P_E = 40 \ MW$.

Now, a reasonable approximation for the amount of current that can be driven per watt of absorbed power is given in terms of the local current drive efficiency $\eta_{CD}$ [30-32]

$$\eta_{CD} = \frac{R_0 \bar{n} I_{CD}}{P_{CD}} \approx \frac{1.2}{n_\parallel^2}$$

$$n_\parallel \approx \frac{\omega_{pe}}{\Omega_e} + \left[ 1 + \frac{\omega_{pe}^2}{\Omega_e^2} \right]^{1/2} \left( 1 - \frac{\omega_{LH}^2}{\omega^2} \right)^{1/2}$$

(31)

where $\omega_{LH}^2(\rho) = \omega_{pi}^2 / (1 + \omega_{pe}^2 / \Omega_e^2)$ is the square of the lower hybrid frequency, $n_\parallel$ is the parallel index of refraction, and the units are $\bar{n}(10^{20} m^{-3})$, $I_{CD}(MA)$, and $P_{CD}(MW)$. We assume that the desired minimum frequency is determined by the strictest of several

constraints corresponding to the avoidance of parametric decay instabilities (PDI). The value for this frequency is given by [30] $\omega \approx 2\omega_{LH}(\rho_m)$ with $\rho_m \approx 0.8$ being the approximate desired location of the peak electron Landau damping for reactor-like temperatures. Also, to evaluate these expressions we set the density $n = n(\rho_m)$ and, for an outside launch, $B = B[R_0(1+\varepsilon\rho_m)] = B_0 / (1+\varepsilon\rho_m)$.

The density $n$ and magnetic field $B_0$ have already been expressed in terms of $a$ from Eq. (25) and the relation $B_0 = B_{max}(1-\varepsilon_B)$. This in turn leads to a straightforward although complicated algebraic relation for $n_{\parallel} = n_{\parallel}(a)$. In the analysis that follows the actual expression for $n_{\parallel}(a)$ is used to numerically evaluate the current drive efficiency. However, for reference case it is worth noting that typically $n_{\parallel} = 1.67$ corresponding to $\eta_{CD} = 0.43 \ MA / MW\text{-}m^2$. Using these reference values it follows that the absorbed RF power can drive a current $I_{CD} = 2.25 \ MA$, which turns out to be only a small fraction of the required current. Lastly, note that by combining the expression for $n_{\parallel}(a)$ with previously derived results we can easily derive an expression for the bootstrap fraction

$$f_B(a) = 1 - \frac{I_{CD}(a)}{I(a)} = 1 - 1.2\frac{P_{CD}}{R_0\overline{n}In_{\parallel}^2} \tag{32}$$

For the reference tokamak, $f_B = 0.84$.

### 4.7 Two additional figures of merit

The design discussion closes with the evaluation of two additional figures of merit, one related to cost and the other to heat flux. The absolute numerical value of these parameters is not very critical. However, they are useful when making comparisons

with the different design options discussed in future sections. The definitions of these parameters are as follows.

- **The cost parameter**

A simple but qualitatively correct measure of cost, originally introduced by Spears and Wesson [33], is the ratio of the volume of highly engineered reactor components to the electric power out. A larger volume of engineered components implies a larger absolute cost. Also, the key parameter is not the absolute cost, but the cost per watt. Hence, the ratio $V_I / P_E$ is introduced as the cost parameter, where $V_I$ includes the volume of the blanket region and the TF coils. A short calculation leads to

$$\frac{V_I}{P_E} = \frac{V_B + V_{TF}}{P_E}$$
$$V_B = 2\pi^2 R_0 \left[ (a+b)(\kappa a + b) - \kappa a^2 \right] \tag{33}$$
$$V_{TF} = 4\pi c \left( 2R_0 - 2a - 2b - c \right)\left[ (1+\kappa)a + 2b + c \right]$$

For the reference reactor we obtain $V_I / P_E = 1.00 \ m^3 / MW$.

- **The heat flux parameter**

In a reactor the alpha power is converted into heat which is eventually lost from the plasma core by means of thermal conduction. This power represents the heat loss from the plasma. It enters the scrape-off layer, largely at the outboard midplane, where it flows essentially parallel to the field and is ultimately dissipated by a combination of expanded contact with the divertor plates and radiation resulting from detachment.

The critical figure of merit is defined by noting that if all the heating power were to be lost by a purely poloidal flow in the scrape-off layer, the corresponding poloidal heat flux in the large aspect ratio limit would be given by $h_p \approx P_\alpha / 2\pi R_0 \lambda_q$ where $\lambda_q$ is the width of the scrape-off layer. Empirical evidence has shown the surprising result that $\lambda_q \propto 1 / B_p$ independent of geometry [34, 35]. Here $B_p$ is the poloidal magnetic field at the outboard midplane.

Now, the heat flux is not lost poloidally, but instead along the magnetic field. Thus, the power that must be safely dissipated is given by $h_\parallel \approx (L_\parallel / 2\pi a) h_p = (R_0 q_a / a) h_p$ with $q_a \approx a B_0 / R_0 B_p$ the edge safety factor. These results can be combined into a simple figure of merit which is a measure of the parallel heat flux that must be dissipated

$$Q_\parallel = \frac{P_\alpha B_0}{R_0} = \left( \frac{E_\alpha}{E_f} \frac{P_E}{\eta_T} \right) \left( \frac{B_0}{R_0} \right) \tag{34}$$

Typical values of $Q_\parallel (MW\text{-}T / m)$ for existing experiments with $P_\alpha$ replaced by $P_{heat}$ are as follows: DIII-D $= 40$, JET $= 45$, Alcator C-Mod $= 65$. For ITER the expected value (using $P_\alpha$) is ITER $= 130$. For recent reactor studies [3] the design requirements are ACT1 $= 390$, ACT2 $= 570$. For the reference design presented here we find $Q_\parallel = 499 \ MW\text{-}T / m$.

## 5. How well does the plasma perform?

We now know what engineering and nuclear physics requires from plasma performance for a standard tokamak reactor. The next question to ask is whether or not the plasma can be expected to meet these requirements assuming its performance is constrained to lie within well-established operational limits determined over years of

experimental operation. To answer this question we focus on four basic tokamak operational limits: (1) the Greenwald density limit, (2) the Troyon beta limit, (3) the kink safety factor disruption limit, and (4) the achievable bootstrap fraction. The comparisons between required and achievable values are discussed in the follow-on subsections.

**5.1 The Greenwald density limit**

The Greenwald limit [36] is given by

$$\bar{n} < \bar{n}_G \equiv \frac{I}{\pi a^2} \tag{35}$$

Substituting numerical values for the reference reactor leads to the requirement that

$$1.43 < 2.56 \qquad \checkmark \tag{36}$$

The Greenwald density limit is satisfied by a substantial safety margin.

**5.2 The Troyon beta limit**

The maximum achievable beta in a tokamak plasma is given by the Troyon limit [37]

$$\beta < \beta_T \equiv \beta_N \frac{I}{aB_0} \qquad \beta_N = 2.8\% \tag{37}$$

After again substituting the reference numerical values we obtain the requirement on $\beta$ that

$$4.13 < 4.39 \quad \checkmark \tag{38}$$

The Troyon beta limit is satisfied but only just barely. There is not much safety margin.

**5.3 The kink safety factor limit**

To avoid current driven major disruptions the kink safety factor must satisfy [38-40]

$$q_* > q_K \approx 2 \tag{39}$$

Substituting values from our reference reactor design yields

$$1.56 > 2 \quad \times \tag{40}$$

The required $q_*$ lies below the minimum achievable value. The plasma current needed to produce the required confinement time is just too large with respect to the allowable current for disruption avoidance. In other words disruption avoidance is a major problem for our standard tokamak reactor. Possible cures for this problem are discussed shortly.

**5.4 The bootstrap fraction**

A short calculation is required to determine the maximum achievable bootstrap fraction. The analysis proceeds as follows. For simplicity we consider a large aspect ratio circular cross section tokamak with minor radius $\hat{a}$. To model elongation we assume that $\hat{a} = \kappa^{1/2}a$ in order to preserve the total cross sectional area. It is also assumed that $T_e = T_i = T$ and $Z = 1$. Under these assumptions the expression for the local neoclassical bootstrap current can be written as [29]

$$
\begin{aligned}
J_B(\rho) &= -2.44\left(\frac{r}{R_0}\right)^{1/2}\left(\frac{p}{B_\theta}\right)\left(\frac{1}{n}\frac{\partial n}{\partial r} + 0.055\frac{1}{T}\frac{\partial T}{\partial r}\right) \\
&= \left[4.88(1+\nu_p)(\nu_n + 0.055\nu_T)\frac{\overline{p}}{\hat{a}^{1/2}R_0^{1/2}}\right]\frac{\rho^{3/2}(1-\rho^2)^{\nu_p-1}}{B_\theta} \\
&= \left[6.8\frac{\overline{p}}{\hat{a}^{1/2}R_0^{1/2}}\right]\frac{\rho^{3/2}(1-\rho^2)^{1/2}}{B_\theta}
\end{aligned}
\tag{41}
$$

Here, $\rho = r/\hat{a}$ and the last two expressions use the profiles given in Eq. (20).

To complete the evaluation of the bootstrap current density the profile of $B_\theta$ resulting from the total current must be specified. Since lower hybrid heating occurs off axis near the plasma edge (i.e. typically $r/\hat{a} \sim 0.8$) we model the total current density $J_T(\rho)$ with the relatively simply expression

$$
J_T(\rho) = \frac{I}{\pi\hat{a}^2}\left(\frac{9\rho^{1/4}}{8}\right)\left[\frac{\alpha^2(1-x)e^{\alpha x}}{e^\alpha - 1 - \alpha}\right]
\tag{42}
$$

where $\rho = x^{4/9}$ and $\alpha = 2.53$. Also, for simplicity we have ignored the need for a seed current on axis. A plot of $J_T(\rho)$ is illustrated in Fig. 4. Equation (42) can be easily integrated yielding the necessary relation for $B_\theta(\rho)$,

$$b_\theta(\rho) = \frac{B_\theta(\rho)}{\mu_0 I / 2\pi \hat{a}} = \frac{1}{\rho}\left[\frac{(1+\alpha-\alpha x)e^{\alpha x} - 1 - \alpha}{e^\alpha - 1 - \alpha}\right] \tag{43}$$

The desired expression for the achievable neoclassical bootstrap fraction is obtained by substituting Eq. (43) into Eq. (41) and then carrying out a simple numerical integration over the plasma cross section.

$$f_{NC} = \frac{I_B}{I} = 268\left(\frac{a^{5/2}\kappa^{5/4}\overline{p}}{\mu_0 R_0^{1/2} I^2}\right)\int_0^1 \left[\frac{\rho^{5/2}(1-\rho^2)^{1/2}}{b_\theta}\right]d\rho \tag{44}$$

To achieve steady state operation the achievable bootstrap fraction must equal or exceed the required bootstrap fraction. This criterion reduces to

$$f_{NC} > f_B \tag{45}$$

which for the reference reactor translates into

$$0.44 > 0.84 \quad \times \tag{46}$$

We see that the criterion is violated by a large margin. A standard tokamak cannot generate a large enough bootstrap current to maintain steady state operation.

**5.5 The overall conclusion with respect to plasma performance**

The analysis has shown that our reference tokamak plasma with standard profiles and a limiting magnetic field at the coil of $B_{max} = 13\ T$ satisfies the Greenwald density limit and the Troyon beta limit. However, the required plasma current violates the kink disruption limit. Equally important, the achievable bootstrap current is far below the

required value for steady state operation. The difficulties with plasma performance all trace back to the need for a high plasma current to achieve a sufficient $\tau_E$ for ignited operation.

The above conclusions have been based on numerical values obtained from the reference design which assumes that $R_0 / a = 4$. The conclusions are in fact more general. To see this we have repeated the entire analysis just presented but now allow $a$ to be a free parameter. We then ask whether or not there is any value of $a$ for which all the plasma physics demands can be simultaneously satisfied.

A convenient way to understand the analysis is illustrated in Fig. 5. Shown here are curves of (a) the required density/Greenwald density $\overline{n} / n_G$, (b) the required beta/Troyon beta $\beta / \beta_T$, (c) the minimum achievable kink safety factor/required kink safety factor $q_K / q_*$, and lastly (d) the required bootstrap fraction/neoclassical bootstrap fraction $f_B / f_{NC}$, all plotted as a function of $a$. Each of these quantities must be simultaneously less than unity (i.e. lie in the unshaded region) for a successful reactor. We see that this can never occur for any value of $a$!

*The conclusion is that the absence of steady state and the excitation of disruptions are potential "show stoppers" for the standard tokamak. Ways must be found to reduce the required current in order resolve these problems. In other words, based on our definition of "standard" there is no zeroth order self-consistent tokamak reactor design that simultaneously accounts for engineering, nuclear physics, and plasma physics.*

This important conclusion was reached independently several years ago by Manheimer [41, 42] also using relatively simple models and what he describes as "conservative design rules". His proposed solution is not to focus on improvements in plasma physics and fusion technology as advocated in the AIRES studies and in the analysis presented here. Instead, his focus is on a potentially less demanding mission – the production of fission fuel by means of a fusion-fission hybrid.

## 6. Possible solutions

We discuss four possible approaches to resolve the problem of too much required current relative to achievable current. The first approach involves advanced plasma physics, the second involves advanced engineering, and the third and fourth involve relaxing a primary engineering constraint. The basic issues are first described qualitatively and then quantified by means of analysis.

### 6.1 The plasma physics approach – raise $H$

The first approach attempts to resolve the problem by means of advanced plasma physics, namely by assuming methods can be developed to increase the achievable energy confinement time. In terms of the analysis this is equivalent to increasing the value of the H-mode enhancement factor $H$. Practically this may be achievable by means of advanced tokamak (AT) operation in which profile control leads to the formation of appropriately located internal and edge transport barriers [43-45]. If successful, this approach has the advantage of leaving the reactor geometry and magnetic field essentially intact – the cost per watt remains unchanged, a major advantage. There is no cost penalty. There are, however, other disadvantages. Raising $H$ lowers $I$, which while good for achieving steady state, is bad for the Greenwald density and Troyon beta limits both of which are lowered. Almost always the Troyon beta limit is violated requiring operation at $\beta_N$ substantially above 2.8%. MHD stability then requires feedback stabilization, a possible but not as yet routine experimental mode of operation. Also, increasing $H$ depends on controlling the current and pressure profiles by means of external power sources. This may become problematic in ignited plasmas because of the dominance of alpha particle heating.

The reactor design analysis for the plasma physics approach is straightforward. The calculations in sections 4 and 5 are repeated treating the H-mode enhancement factor $H$ as a free parameter. For each value of $H$ the plasma radius $a$ is chosen so that required bootstrap fraction is equal to the achievable bootstrap fraction: $f_B = f_{NC}$. This additional constraint leads to a unique value of $a$ for the given value of $H$. Once this critical $a = a(H)$ is determined, the plasma performance criteria can be evaluated. The goal is to see whether or not there are values of $H$ for which all plasma performance criteria are satisfied.

The results of this analysis are illustrated in Fig. 6. Shown here are curves, all for $B_{max} = 13\ T$, similar to Fig. 5 with $H$ now the variable along the horizontal axis. Recall that each of these quantities must be simultaneously less than unity (i.e. lie in the unshaded region) for a successful reactor.

We see, unfortunately, that there is no value of $H$ for which all the remaining plasma performance criteria are simultaneously satisfied. Specifically, $H = 1.26$ is the lowest enhancement factor at which the kink stability criterion is satisfied. At this value the Greenwald limit is still satisfied. However, the Troyon limit is now violated. To resolve this problem the allowable beta limit, as defined by $\beta_N$, would also need to be increased, by a factor of 1.29; that is, $\beta_N$ must increase from 2.8 % to 3.6 %. Further increases in $H$ only make things worse as the beta limit is even further violated. Also the required enhancements in $H$ and $\beta_N$ are found to be noticeably larger than the above values in more realistic designs that include safety margins [3]. For instance the ACT-1 advanced tokamak design requires $H = 1.65$ and $\beta_N = 4.7$.

Note also that at $H = 1.26$ the two figures of merit have the values $V_I / P_E = 1.07\ m^3 / MW$ and $Q_{\parallel} = 507\ MW\text{-}T / m$. Both of these values are essentially identical to the reference case. As anticipated there is no penalty in either cost or heat load for the advanced plasma physics option.

To summarize, a tokamak reactor based on advanced plasma physics requires an enhancement in both energy confinement and beta accompanied by robust engineering reliability. This may be possible with continued research but in the authors' view this is a risky strategy if it is the only one upon which the future of the tokamak concept is based.

## 6.2 The engineering approach – raise $B_{max}$

The second approach to the bootstrap issue involves advances in engineering, specifically, raising the maximum allowable magnetic field at the inside of the TF coil. Raising $B_{max}$ lowers the required plasma current and raises the current drive efficiency, both important advantages. Higher field also makes it easier to satisfy the kink disruption limit and the Troyon beta limit. It only weakly affects the Greenwald density limit. With higher magnetic field plasma performance becomes more robust, perhaps not surprisingly since it is "magnetic fusion".

From a practical point of view the science component of higher field has already been demonstrated – high temperature superconductors (e.g. YBCO) operating at about $4.2\,°K$ have critical fields well above $20\,T$ at current densities of reactor interest [46]. What is needed is an engineering R&D program to transform these high temperature superconductors into large fusion magnets capable of supporting high mechanical stresses. The main disadvantage of increasing $B_{max}$ is that substantially more structural material is needed to support these stresses leading to an increased volume for the TF magnets. Thus, there can be a substantial cost penalty incurred by the use of higher field magnets as compared to the advanced plasma physics approach.

The analysis of the high $B_{max}$ option also closely follows the analysis presented in sections 4 and 5 with one important difference. Recall that in the reference case a value of $B_0$ is specified such that $B_{max}$ at the coil is ultimately set equal to its maximum

allowable value of $13\ T$: $B_0 = B_{\max}(1 - \varepsilon_B)$. The analysis presented in this section is identical except that $B_{\max}$ is treated as a free parameter (with $H$ fixed at unity). The goal is to determine whether a higher value of $B_{\max}$ can be found such that all the plasma physics requirements can be satisfied holding $H = 1$. As for the advanced plasma physics case, the required bootstrap fraction is set equal to the achievable bootstrap fraction as an additional constraint to uniquely determine the value of $a = a(B_{\max})$.

The results from these calculations are illustrated in Fig. 7. The first set of curves presented in Fig. 7a is similar to Fig. 5 except that the horizontal axis is now $B_{\max}$. From these curves we see that high field, as expected, does indeed lead to improved plasma performance. An important conclusion is that when $B_{\max} \geq 17.6\ T$ all the plasma physics constraints are simultaneously satisfied, with the kink stability limit being the most difficult requirement.

However, as stated, this success does not come without a price. The higher field requires substantially more structure which in turn increases the cost function. This behavior is illustrated in Fig. 7b where we have plotted $V_I / P_E$ versus $B_{\max}$. Observe that the cost function is an increasing function of $B_{\max}$. Its value has increased from $1.07\ m^3 / MW$ for the advanced physics case at $B_{\max} = 13\ T$ to $1.87\ m^3 / MW$ at $B_{\max} = 17.6\ T$. The cost function $V_I / P_E$ has increased by a factor of about 1.75. The overall cost penalty is substantial.

Lastly note that at $B_{\max} = 17.6\ T$ the heat flux parameter has the value $Q_\parallel = 657\ MW\text{-}T/m$. This is an increase of a factor 1.30 over the advanced physics case. The penalty is not as large as for the cost parameter but it is still significant.

In summary, high field enables all the plasma physics constraints to be simultaneously satisfied although with a substantial cost penalty. Still, it makes good sense to develop high field magnets since without increasing $B_{\max}$ it is not possible to simultaneously satisfy all the plasma physics constraints except by means of yet to be

proven plasma physics advancements. Also, as high field magnets are developed, engineering innovation may possibly lead to lower cost ways to manufacture such magnets, thereby reducing the cost penalty.

**6.3 Relaxing the power output constraint – raise $P_E$**

The next option considered to alleviate the steady state problem is to relax one of the main engineering constraints used in the reactor design. Namely, in this option we allow the total power output of the plant to be greater than $P_E = 1000 \ MW$. Higher power ultimately leads to improved performance because of well-known economy of scale arguments. The disadvantages of larger power output are also well-known. Higher power increases the overall risk of grid instability by having too much output concentrated in one plant. Also, while the cost per watt may not change very much the absolute capital cost will increase since the total power has increased, thereby representing a disincentive to investors. Still, it is of interest to learn how much the output power must be increased in order for all the plasma physics constraints to be simultaneously satisfied.

The analysis for the high $P_E$ option is carried out as follows. We fix $H = 1$, $B_{max} = 13 \ T$ and again require that $f_B = f_{NC}$ to uniquely determine $a = a(P_E)$. These requirements are similar to the $B_{max}$ option except that now $B_{max}$ is held fixed while $P_E$ is allowed to vary.

The results are shown in Fig. 8a which again illustrates the ratios of required to achievable plasma parameters as a function of $P_E$. Observe that the minimum value of power for which all plasma criteria are simultaneously satisfied is $P_E = 1550 \ MW$. At this value, coincidentally, the kink and beta limits are each marginally satisfied simultaneously. The Greenwald limit is satisfied by a safe margin.

Figure 8b illustrates the corresponding curve of $V_I / P_E$ versus $P_E$. Note that $V_I / P_E$ is a strongly decreasing function of $P_E$. At the value $P_E = 1550 \ MW$ we find that $V_I / P_E = 1.17 \ m^3 / MW$. This is nearly the same as the advanced plasma physics design for which $V_I / P_E = 1.07 \ m^3 / MW$. In other words there is not much of a cost penalty in the trade-off between increased power output versus advanced plasma physics. This is the benefit of economy of scale. On the other hand the value of the heat flux parameter at $P_E = 1550 \ MW$ is $Q_\parallel = 673 \ MW\text{-}T/m$ which is significantly higher than the $Q_\parallel = 507 \ MW\text{-}T/m$ value for the advanced physics design.

To summarize, by considering a reactor with $P_E > 1000 \ MW$ it is possible to develop a design which simultaneously satisfies all plasma physics constraints. This design does not require advanced plasma physics (i.e. $H = 1$) or new superconducting magnet development (i.e. $B_{max} = 13 \ T$). The downsides are the large power output and the high absolute capital cost even though the cost per watt is nearly unchanged from the advanced physics value..

## 6.4 Relaxing the wall loading constraint – lower $P_W$

The final option of interest considers the possibility of operating at a lower neutron wall loading limit than the standard value of $P_W = 4 \ MW / m^2$. In general a lower $P_W$ limit reduces the required plasma pressure, thereby easing many of the plasma physics demands. This should make it easier to simultaneously satisfy the four basic demands on plasma performance. The downside of reducing $P_W$ is also well known. The resulting lower plasma pressure corresponds to a lower fusion plasma density. Consequently, a large plasma volume is needed to produce the same total output power, which translates into a higher cost per watt. This is the main disadvantage of the low $P_W$ strategy. The goal of the analysis that follows is to see how much lower $P_W$ must

become so that all plasma requirements are simultaneously satisfied and to calculate the corresponding increase in the cost per watt figure of merit.

The details of the analysis are very similar to the $P_E$ option. We fix $B_{max} = 13 \ T$, $H = 1$, $P_E = 1000 \ MW$ and allow $P_W$ to be a free parameter. Also we again set $f_B = f_{NC}$ as an additional constraint to uniquely determine $a = a(P_W)$.

The results are illustrated in Fig. 9. In Fig. 9a the plasma performance requirements are plotted vs. $P_W$. Observe that all the requirements are simultaneously satisfied when $P_W \leq 2.1 \ MW \ / \ m^2$ with the kink limit being the strictest. The question now is how high is the cost penalty? This is addressed in Fig. 9b which illustrates $V_I \ / \ P_E$ vs. $P_W$. The cost increases rapidly as $P_W$ decreases. The $V_I \ / \ P_E$ penalty is substantial, increasing from $V_I \ / \ P_E = 1.07 \ m^3 \ / \ MW$ for the advanced physics design to $V_I \ / \ P_E = 2.59 \ m^3 \ / \ MW$ for the $P_W = 2.1 \ MW \ / \ m^2$ design, a factor of about 2.42. In contrast, the heat flux parameter decreases from the advanced tokamak value $Q_{\parallel} = 507 \ MW\text{-}T/m$ to $Q_{\parallel} = 374 \ MW\text{-}T/m$ for the low $P_W$ design. The heat flux problem is substantially reduced, not a surprising result since the plasma power density is lower.

In summary, by considering a reactor with $P_W < 4 \ MW \ / \ m^2$ it is possible to develop a design which simultaneously satisfies all plasma physics requirements. No advanced plasma physics is required,(i.e. $H = 1$) nor new superconducting magnet development (i.e. $B_{max} = 13 \ T$). Also, the power output remains at $P_E = 1000 \ MW$. The downside is the large increase in the cost figure of merit.

## 6.5 Final designs

For reference we summarize below in Table 3 the critical distinguishing design parameters for the reference reactor and those of the four options.

| Quantity | Reference $B_{\mathrm{max}} = 13$ | Option 1 $H = 1.26$ | Option 2 $B_{\mathrm{max}} = 17.6$ | Option 3 $P_E = 1554$ | Option 4 $P_W = 2.1$ |
|---|---|---|---|---|---|
| $B_{\mathrm{max}}\ (T)$ | 13 | 13 | 17.6 | 13 | 13 |

| $H$ | 1 | 1.26 | 1 | 1 | 1 |
|---|---|---|---|---|---|
| $P_E$ $(MW)$ | 1000 | 1000 | 1000 | 1554 | 1000 |
| $P_W$ $MW \, / \, m^2$ | 4 | 4 | 4 | 4 | 2.1 |
| $V_I \, / \, P_E \, (m^3 \, / \, MW)$ | 1.00 | 1.07 | 1.87 | 1.17 | 2.59 |
| $Q_{\parallel}$ $(MW\text{-}T/m)$ | 499 | 507 | 657 | 673 | 374 |
| $B_0$ $(T)$ | 6.83 | 7.36 | 12.4 | 8.54 | 9.74 |
| $a$ $(m)$ | 1.34 | 1.26 | 0.97 | 1.44 | 1.35 |
| $c$ $(m)$ | 0.97 | 0.98 | 1.64 | 1.07 | 1.12 |
| $R_0$ $(m)$ | 5.34 | 5.57 | 7.39 | 7.70 | 10.2 |
| $R_0 \, / \, a$ | 4.00 | 4.5 | 7.65 | 5.34 | 7.51 |
| $\overline{p}$ $(atm)$ | 7.57 | 7.79 | 8.90 | 7.29 | 5.42 |
| $\overline{n}$ $(10^{20} m^{-3})$ | 1.43 | 1.47 | 1.68 | 1.37 | 1.02 |
| $\overline{n} \, / \, n_G$ | 0.56 | 0.73 | 0.64 | 0.80 | 0.69 |
| $\tau_E$ (sec) | 0.94 | 0.91 | 0.80 | 0.97 | 1.31 |
| $I$ $(MA)$ | 14.3 | 10.0 | 7.64 | 11.2 | 8.52 |
| $\beta$ (%) | 4.13 | 3.66 | 1.46 | 2.54 | 1.46 |
| $\beta \, / \, \beta_T$ | 0.94 | <mark>1.21</mark> | 0.82 | 1.00 | 0.80 |
| $q_*$ | 1.56 | 2.00 | 2.00 | 2.00 | 2.00 |
| $q_K \, / \, q_*$ | <mark>1.28</mark> | 1.00 | 1.00 | 1.00 | 1.00 |
| $f_B$ | 0.84 | 0.78 | 0.69 | 0.70 | 0.66 |
| $f_B \, / \, f_{NC}$ | <mark>1.90</mark> | 1.00 | 1.00 | 1.00 | 1.00 |

Table 3  Final design parameters for the reference reactor and options 1, 2, 3, and 4.
Highlighted quantities violate achievable plasma physics values.

## 7. Discussion

The analysis presented here has shown that a tokamak with standard profiles and existing technology does not scale to a 1000 $MW$ power producing reactor. The source of the problem is that the required current to produce a long enough confinement time for ignited operation is simply too high. This high current substantially exceeds the achievable current drive plus bootstrap plus current thereby preventing steady state operation. It also leads to violation of the MHD kink stability criterion implying the excitation of major disruptions.

Several strategies have been suggested to overcome the high current difficulty. Qualitatively, if one could improve both the achievable confinement time (i.e. raise $H$ ) and the MHD beta limit (i.e. raise $\beta_N$ ) all plasma physics requirements, by definition, could be simultaneously satisfied. This is option 1. The problem is that this is very difficult to do experimentally particularly with the robustness necessary for a reactor. However, in the context of our simple model there is essentially no cost penalty if this strategy is successful.

A second approach, corresponding to options 2, holds the plasma physics constant but allows for a higher magnetic field at the coil, on the order of $18\,T$ . High temperature superconductors such as YBCO can already achieve this goal but an engineering R&D program is needed to develop large scale magnets for fusion applications. At high magnetic fields it becomes progressively easier to simultaneously satisfy the plasma physics constraints. It is the authors' belief that the high field approach has a higher probability of success than the advanced plasma physics strategy. Even so, we must recognize that in a reactor, higher field may well lead to a significant cost penalty compared to the advanced plasma strategy.

The third approach is option 3 in which the plasma physics and magnet technology are held fixed at present values (i.e. $H = 1$, $B_{max} = 13\,T$ ) but the power output is increased to about $P_E \approx 1500\,MW$ . With this approach all plasma physics and magnet constraints are satisfied with existing technology. There is only a small cost penalty,

although one must decide if such a large power plant makes sense with respect to grid stability and investor attractiveness.

The fourth and final approach, holds the plasma physics, magnet technology, and power output fixed at present day values (i.e. $H = 1$, $B_{max} = 13 \ T$, $P_E = 1000 \ MW$) but allows the neutron wall loading to be reduced. When $P_W \approx 2 \ MW \ / \ m^2$ all plasma requirements can be simultaneously satisfied. The main disadvantage is that lower wall loading leads to a higher cost per watt.

Lastly, we must accept the possibility that the problem of achieving a sufficiently high current in a tokamak for ignited operation, consistent with current drive and bootstrap current constraints, may be just too difficult to achieve scientifically and/or technologically. As such, it makes sense to have strong and serious backup alternatives. Two such alternatives are the stellarator [47 – 49] and the fusion-fission hybrid [50].

Since a stellarator does not require a net toroidal current for steady state operation this is a major scientific advantage. The only current that flows is the natural bootstrap current. It is also possible to design a stellarator such that even this natural bootstrap current is minimized. The key point is that no toroidal current must be driven externally. A further important advantage is that with only a small or nearly zero bootstrap current, stellarators rarely if ever experience major disruptions.

Counteracting these advantages are two problems. First, the 3-D geometry of a stellarator can cause neoclassical heat transport to exceed even the expected turbulent transport. The principle of quasi-symmetry can be used to reduce neoclassical transport but this is still an area of active research. The second problem is the added technological complexity of 3-D stellarator magnets as compared to relatively simple flat coils of a tokamak. This too is an area of active engineering research.

The second alternative to the steady state tokamak is the fusion-fission hybrid. The motivation here is that a fusion reactor will likely be more expensive than a light water fission reactor. The reason is fusion's low power density which ultimately leads to large

size and large cost. To overcome this economic competition it may therefore make sense to increase the focus on fissile fuel production using fusion-fission hybrids as advocated for many years by Manheimer [41, 42]. Another hybrid application is the burning of radioactive waste [51]. For a hybrid, the plasma physics may be less demanding and the large cost is highly leveraged among the 5 or so fission reactors for which either fuel is being provided or waste is being burned. However, the engineering requirements of a hybrid may be of comparable or even greater difficulty because of the need for a complicated fission blanket.

In the end the desirability of a hybrid will be strongly tied to economics. For both fuel production and waste burning the fission community has offered its own solution – the fast burner/breeder [52, 53]. In terms of the economics a hybrid has better chance to compete against this more complex and expensive fission reactor than against a direct power producing light water reactor.

Even so, fission solutions are not the only competition for hybrids. For waste management there is the possibility of underground repositories [54] (such as Yucca Mountain) or burial in deep bore holes [55]. These may be inherently less expensive – "dig a hole" vs. build a super high tech facility.

For fuel production the competition is even more striking. There is sufficient uranium in the ocean to provide a virtually limitless supply of uranium for light water reactors. Techniques have already been developed to extract this uranium on a small to moderate scale at a cost that may be hard to beat [56]. The problem here is that astoundingly large amounts of ocean water would need to be processed every year to generate enough uranium to supply the world's light water reactors. Still, the technology is here and at some scale, already works.

Based on these observations the authors are led to believe that a logical, common sense strategy for the US fusion program should include the following components.

1. A strong experimental and theoretical program aiming to improve plasma confinement and MHD beta limits in connection with the advanced physics option.

2. An experimental demonstration that a combination of some form of current drive plus neoclassical bootstrap current in a high density, high field tokamak, can indeed be relied upon to generate steady state operation

3. A high field R&D program whose goals are to (1) produce $20\,T$ magnets using high temperature superconductors and (2) develop demountable joints which would greatly simplify construction and maintenance.

4. Acknowledge that the problem with high current in a tokamak may be just too difficult to overcome scientifically and/or technologically. As such, it makes sense to have a strong and serious stellarator program as a viable backup.

5. Acknowledge that even if all the science and engineering problems are resolved, a fusion reactor may likely still be considerably more expensive than a light water fission reactor. It thus makes sense to increase the focus on fissile fuel production or waste burning using fusion-fission hybrids, keeping in mind the economic competition with other fission and non-fission alternatives.

Unfortunately, only Point 1 and marginally Point 2 presently receive the necessary attention in the US fusion program.

**Figure Captions**

Figure 1 Simple model for the reactor geometry.

Figure 2 Planar model for the blanket region including the first wall, blanket, shield, and vacuum chamber.

Figure 3 (a) Upper half of the TF magnet illustrating the balance between the expansion force and the tensile forces; (b) Inner wedge section of the TF magnet showing the balance between the centering force and the compression forces.

Figure 4 Plot of the total plasma current density $J_T(\rho)$ versus minor radius $\rho = r / a$ for $\alpha = 2.53$ used in the calculation of the bootstrap current.

Figure 5 Curves of $\overline{n} / n_G$, $\beta / \beta_T$, $q_K / q_*$, and $f_B / f_{NC}$ as a function of $a$ for $H = 1$ and $B_{max} = 13\ T$. Successful operation corresponds to the unshaded region.

Figure 6 Curves of $\overline{n} / n_G$, $\beta / \beta_T$, and $q_K / q_*$ as a function of $H$ for $B_{max} = 13\ T$ assuming that $f_B / f_{NC} = 1$. Successful operation corresponds to the unshaded region.

Figure 7 (a) Curves of $\overline{n} / n_G$, $\beta / \beta_T$, and $q_K / q_*$ as a function of $B_{max}$ for $H = 1$ assuming that $f_B / f_{NC} = 1$. Successful operation corresponds to the unshaded region. (b) Corresponding curve of $V_I / P_E$ versus $B_{max}$.

Figure 8 (a) Curves of $\overline{n} / n_G$, $\beta / \beta_T$, and $q_K / q_*$ as a function of $P_E$ for $H = 1$, $B_{max} = 13\ T$ assuming that $f_B / f_{NC} = 1$. Successful operation corresponds to the unshaded region. (b) Corresponding curve of $V_I / P_E$ versus $P_E$.

Figure 9 (a) Curves of $\overline{n} / n_G$, $\beta / \beta_T$, and $q_K / q_*$ as a function of $P_W$ for $H = 1$, $B_{max} = 13\ T$, $P_E = 1000\ MW$ assuming that $f_B / f_{NC} = 1$. Successful operation corresponds to the unshaded region. (b) Corresponding curve of $V_I / P_E$ versus $P_W$.

# References

[1] Najmabadi F, Conn R W, Cooke P I H, Grotz S P, Hasan M Z, Ibrahim E, Kunugi T, Mau T-K, Martin R C, Sharafat S *et al* 1991 *The ARIES-I tokamak reactor study - Final Report*, UCLA-PPG-1323

[2] Najmabadi F, The ARIES Team: Abdou A, Bromberg L, Brown T, Chan V C, Chu M C, Dahlgren F, El-Guebaly L, Heitzenroeder P, Henderson D *et al* 2006 *Fusion Engineering and Design* **80** 3

[3] Kessel C E, Tillack M S, Najmabadi F, Poli F M, Ghantous K, Gorelenkov N, Wang X R, Navaei D, Toudeshki H H, Koehly C *et al* 2013 *ARIES-ACT* http://aries.ucsd.edu/ARIES/DOCS/FST2013/

[4] Maisonnier D, Cook I, Sardain P, Boccaccini L, Di Pace L, Giancarli L, Norajitra P, Pizzuto A, PPCS Team 2006 *Fusion Engineering and Design* **81** 1123

[5] Maisonnier D, Campbell D, Cook I, Di Pace L, Giancarli L, Hayward J, Li Puma A, Medrano M, Norajitra P, Roccella M, Sardain P, Tran M Q, Ward D 2007 *Nuclear Fusion* **47** 1524–1532

[6] Kikuchi M 1990 *Nuclear Fusion* **30** 265

[7] Kikuchi M, Seki Y, Nakagawa K 2000 *Fusion Engineering and Design* **48** 265–270

[8] Nishio S, Ushigusa K, Ueda S, Polevoi A, Tobita K, Kurihara R, Aoki I, Okada H, Hu G, Konishi S *et al* 2002 *Purazuma, Kaku Yugo Gakkai-Shi* **78** 1218-1230

[9] Kotschenreuther M, Valanju P M, Mahajan S M, Wiley J C 2007 Physics of Plasmas **14** 072502

[10] Covele B, Valanju P, Kotschenreuther M, Mahajan S 2014 *Nuclear Fusion* **54** 072006

[11] Ryutov D D 2007 *Physics of Plasmas* **14** 064502

[12] Couture P, Boileau A, Décoste R, Gregory B, Janicki C, Lachambre J-L, Lafrance D, Michaud D, Ross G G, Stansfield B *et al* 1992 *Physics Letters A* **163** 204-208

[13] Petrie T W, Brooks N H, Fenstermacher M E, Groth M, Hyatt A W, Isler R C, Lasnier C J, Leonard A W, Porter G D, Schaffer M J *et al* 2008 *Nucl. Fusion* **48** 045010

[14] Huang J, Feng Y, Wan B, Liu S, Chang J, Wang H, Gao W, Zhang L, Gao W, Chen Y *et al* 2014 *Plasma Phys. Control. Fusion* **56** 075023

[15] Kikuchi M, Fasoli A, Takizuka T, Diamond P, Medvedev S, Duan X, Zushi H, Furukawa M, Kishimoto Y, Wu Y *et al* 2014 *1$^{st}$ International e-Conference on Energies* E002

[16] Nygren R E, Harjes H C, Wakeland P, Ellis R, Kugel H W, Kaita R, Berzak L, Zakharov L, Ehrhart B 2009 *Fusion Engineering and Design* **84** 1438

[17] Federici G, Kemp R, Ward D, Bachmann C, Franke T, Gonzalez S, Lowry C, Gadomska M, Harman J, Meszaros B, Morlock C, Romanelli F, Wenninger R 2014 *Fusion Engineering and Design* **89** 882

[18] Whyte D Paper in preparation, slides available from PSFC seminar 2015 *Fusion Economics & Power Density: Why ADX is Needed*

[19] Zohm H 2101 *Fusion Science and Technology* **58** 613

[20] Sborchia C, Fu Y, Gallix R, Jong C, Knaster J, Mitchell N 2008 *IEEE Transactions on Applied Superconductivity* **18** 463

[21] Sorbom B, Ball J, Palmer T R, Mangiarotti F J, Sierchio J M, Bonoli P, Kasten C, Sutherland D A, Barnard H S, Haakonsen C B *et al* 2014 submitted to *Fusion Engineering Design* "ARC: A compact, high-field, fusion nuclear science facility and demonstration power plant with demountable magnets"

[22] Lao L L and Jensen T H 1991 *Nuclear Fusion* **31** 1909

[23] Raffray A R, Akiba M, Chuyanov V, Giancarli L, Malang S 2002 *Journal of Nuclear Materials* **307–311** 21–30

[24] Ihli T, Basu T K, Giancarli L M, Konishi S, Malang S, Najmabadi F, Nishio S, Raffray A R, Rao C V S, Sagara A, Wu Y 2008 *Fusion Engineering and Design* **83** 912–919

[25] Chadwick M B, Herman M, Obložinský P, Dunn M E, Danon Y, Kahler A C, Smith D L, Pritychenko B, Arbanas G, Arcilla R *et al* 2011 *ENDF/B-VII.1: Nuclear Data for Science and Technology: Cross Sections, Covariances, Fission Product Yields and Decay Data*, Nucl. Data Sheets **112** 2887

[26] See for instance Abdou M A, Morley N B, Ying A Y, Smolentsev S, Calderoni P 2005 *Nuclear Engineering and Technology* 37 401 and references therein

[27] Montgomery D B 1969 *Solenoid Magnet Design* (New York: Robert E. Krieger Publishing Co.)

[28] Thome R J, Tarrh J M 1982 *MHD and fusion magnets* (New York: John Wiley & Sons, Inc.)

[29] See for instance Wesson J 2011 *Tokamaks 4th Edition* (Oxford: Oxford University Press)

[30] Porkolab M 1977 *Physics of Fluids* **20** 2058

[31] Kikuchi M, Lackner K, and Tran M Q 2012 *Fusion Physics* Chapter 6 (Vienna: IAEA)

[32] Also, see for instance Freidberg J 2007 *Plasma Physics and Fusion Energy* Chapter 15 (New York: Cambridge University Press)

[33] Spears W R and Wesson J A 1980 *Nuclear Fusion* **20** 1525

[34] Eich T, Leonard A W, Pitts R A, Fundamenski W, Goldston R J, Gray T K, Herrmann A, Kirk A, Kallenback A, Kardaun O *et al* 2013 *Nuclear Fusion* **53** 093031

[35] LaBombard B, Terry J L, Hughes J W, Brunner D, Payne J, Reinke M L, Cziegler I, Granetz R, Greenwald M, Hutchinson I H *et al* 2011 *Physics of Plasmas* **18** 056104

[36] Greenwald M, Terry J L, Wolfe S M, Ejima S, Bell M G, Kaye S M, Neilson G H 1988 *Nuclear Fusion* **28** 2199

[37] Troyon F, Gruber R, Saurenmann H, Semenzato S, Succi S 1984 *Plasma Physics and Controlled Fusion* **26(1A)** 209

[38] Wesson J A 1978 *Nuclear Fusion* **18** 87

[39] See also Menard J E, Bell M G, Bell R E, Gates D A, Kaye S M, LeBlanc B P, Maingi R, Sabbagh S A, Soukhanovskii V, Stutman D, NSTX National Research Team 2004 *Physics of Plasmas* **11** 639

[40] Shafranov VD 1970 *Soviet Physics-Technical Physics* **15** 175

[41] Manheimer W 2009 *Journal of Fusion Energy* **28** 60

[42] Manheimer W 2014 *Journal of Fusion Energy* **33** 199

[43] Stambaugh R D, Wolfe S M, Hawryluk R J, Harris J H, Biglari H, Prager S C, Goldston R J, Fonck R J, Ohkawa T, Logan B G, Oktay E 1990 *Physics of Fluids* **B2** 2941

[44] Connor J W, Fukuda T, Garbet X, Gormezano C, Mukhovatov V, Wakatani M, the ITB Database Group, the ITPA Topical Group on Transport and Internal Barrier Physics 2004 *Nuclear Fusion* **44** R1 – R49

[45] Hubbard A E 2000 *Plasma Physics and Controlled Fusion* **42** A15

[46] Lee P J 2014 *A comparison of superconducting critical currents* http://fs.magnet.fsu.edu/~lee/plot/plot.htm

[47] Wakatani M 1998 *Stellarator and Heliotron Devices* (Oxford University Press)

[48] Boozer A 2005 *Reviews of Modern Physics* **76** 1071

[49] Helander P, Beidler C D, Bird T M, Drevlak M, Feng Y, Hatzky R, Jenko F, Kleiber R, Proll J H E, Turkin Y, Xanthopoulos P 2012 *Plasma Physics And Controlled Fusion* **54** 124009

[50] Report of the Research Needs Workshop (ReNeW) 2000 *Research Needs for Fusion-Fission Hybrid Systems* (Gaithersburg, Maryland)

[51] Kotschenreuther M, Valanju P M, Mahajan S M, Schneider E A, 2009 *Fusion Engineering and Design* **84** 83-88

[52] Waltar A E, Reynolds A B 1981 *Fast breeder reactors* (New York: Pergamon Press)

[53] Deutch J M, Moniz E J, co-chairs 2003 *The Future of Nuclear Power – An Interdisciplinary MIT Report* (Massachusetts Institute of Technology)

[54] International Atomic Energy Agency 2003 *Scientific and Technical Basis for the Geological Disposal of Radioactive Wastes* Technical Report Series 413

[55] U.S. Nuclear Waste Technical Review Board 2013 *Deep Borehole Disposal of Spent Nuclear Fuel and High-Level Waste*

[56] Seko N, Katakai A, Hasegawa S, Tamada M, Kasai N, Takeda H, Sugo T, Saito K 2003 *Nuclear Technology* **144**(2) 274-278

Figure 1 Simple model for the reactor geometry.
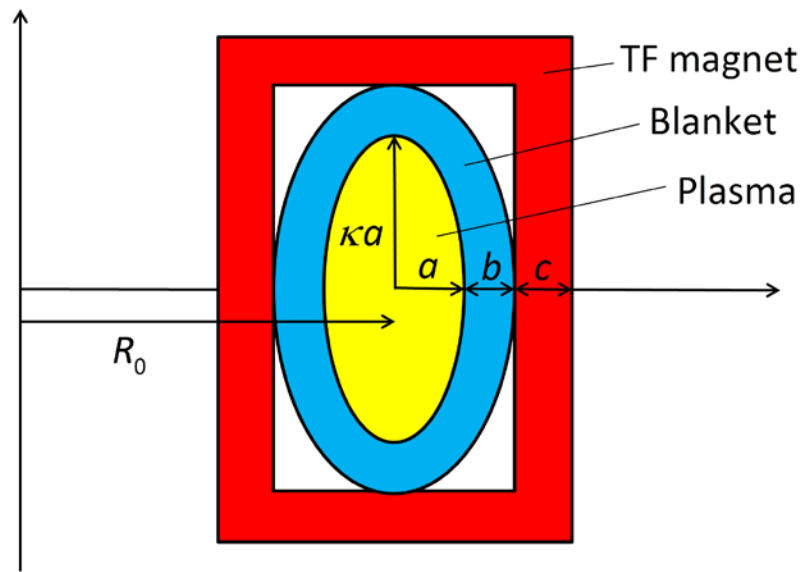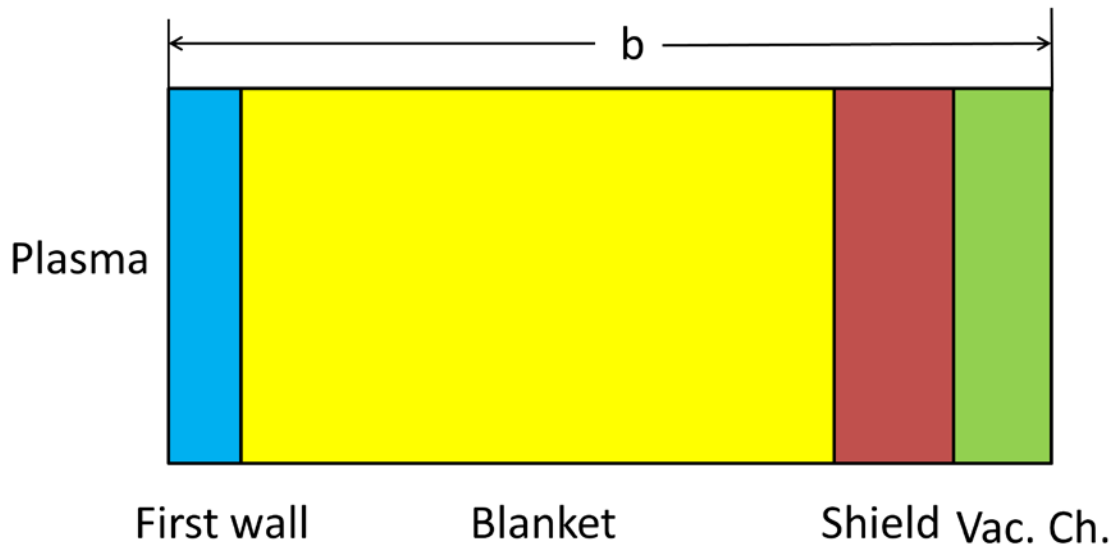


Figure 2 Planar model for the blanket region including the first wall, blanket, shield, and vacuum chamber.
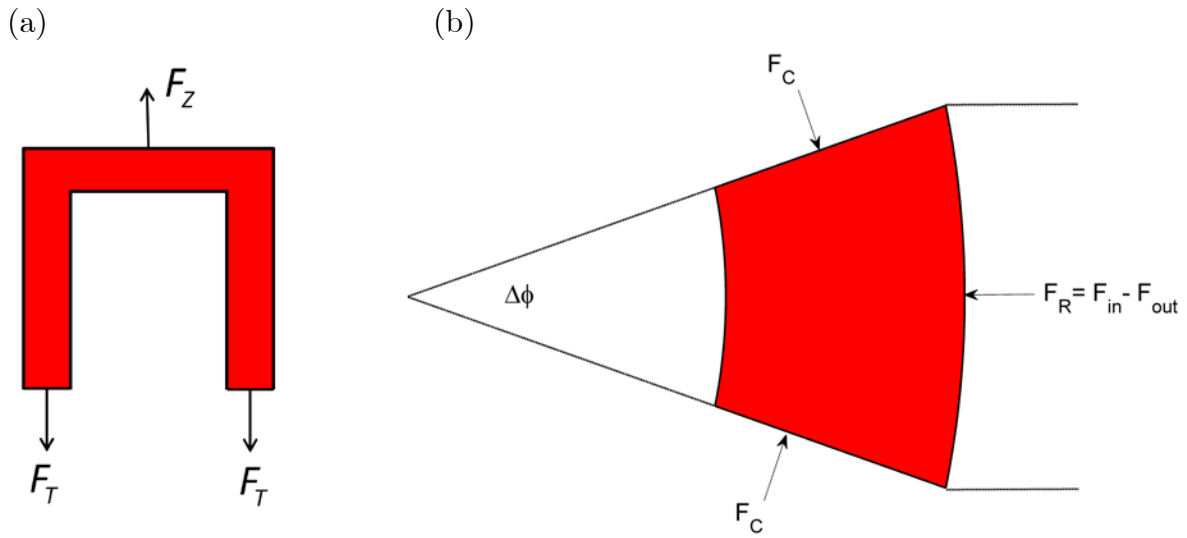
Figure 3 (a) Upper half of the TF magnet illustrating the balance between the expansion force and the tensile forces; (b) Inner wedge section of the TF magnet showing the balance between the centering force and the compression forces.
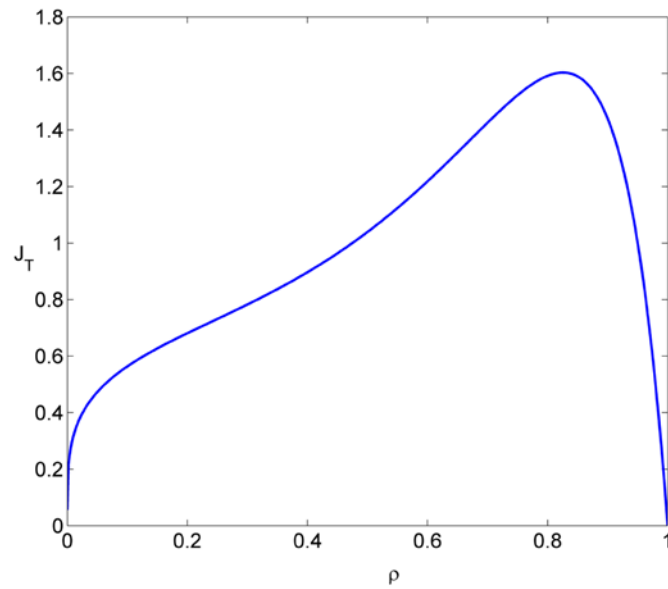


Figure 4 Plot of the total plasma current density $J_T(r)$ versus minor radius $r = r/a$ for $a = 2.53$ used in the calculation of the bootstrap current.
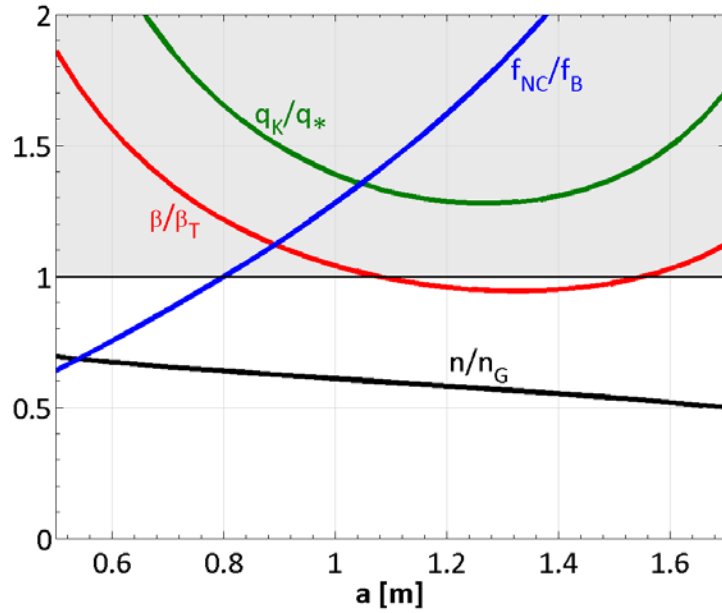
Figure 5 Curves of $\bar{n}/n_G$, $b/b_T$, $q_K/q_*$, and $f_B/f_{NC}$ as a function of $a$ for $H = 1$ and $B_{max} = 13\ T$. Successful operation corresponds to the unshaded region.
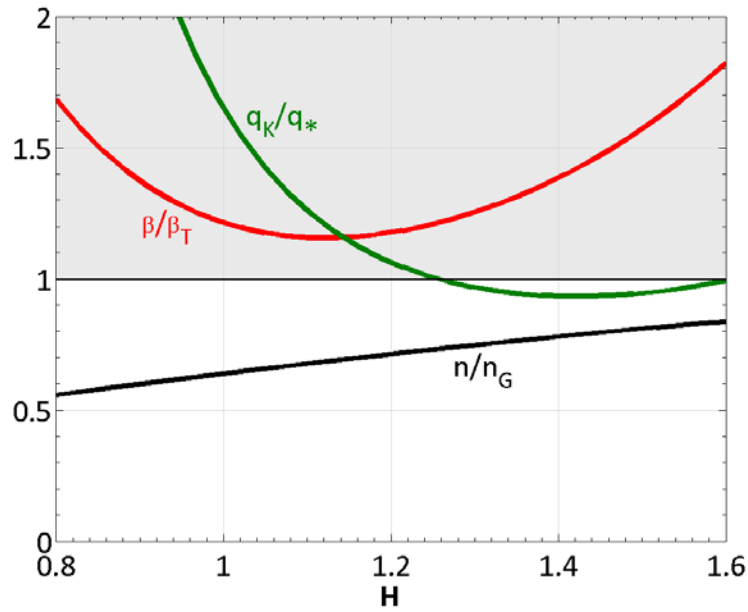


Figure 6 Curves of $\bar{n}/n_G$, $b/b_T$, and $q_K/q_*$ as a function of $H$ for $B_{max} = 13\ T$ assuming that $f_B/f_{NC} = 1$. Successful operation corresponds to the unshaded region.
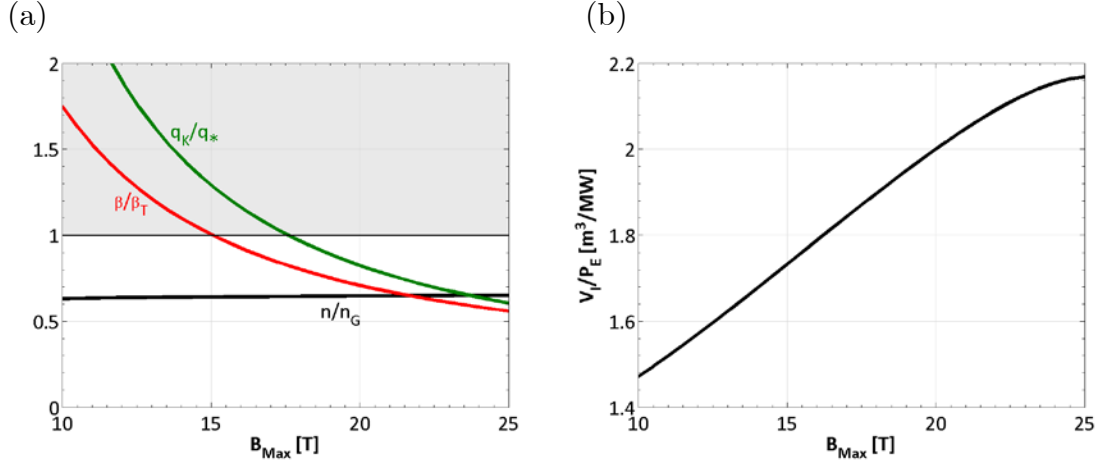
Figure 7 (a) Curves of $\bar{n} / n_G$, $b / b_T$, and $q_K / q_*$ as a function of $B_{max}$ for $H = 1$ assuming that $f_B / f_{NC} = 1$. Successful operation corresponds to the unshaded region. (b) Corresponding curve of $V_I / P_E$ versus $B_{max}$.
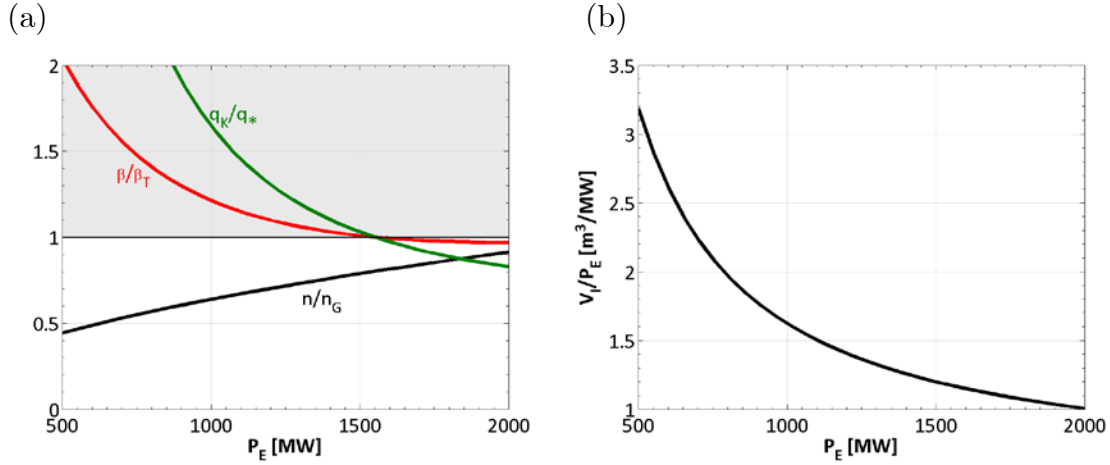


Figure 8 (a) Curves of $\bar{n} / n_G$, $b / b_T$, and $q_K / q_*$ as a function of $P_E$ for $H = 1$, $B_{max} = 13\,T$ assuming that $f_B / f_{NC} = 1$. Successful operation corresponds to the unshaded region. (b) Corresponding curve of $V_I / P_E$ versus $P_E$.
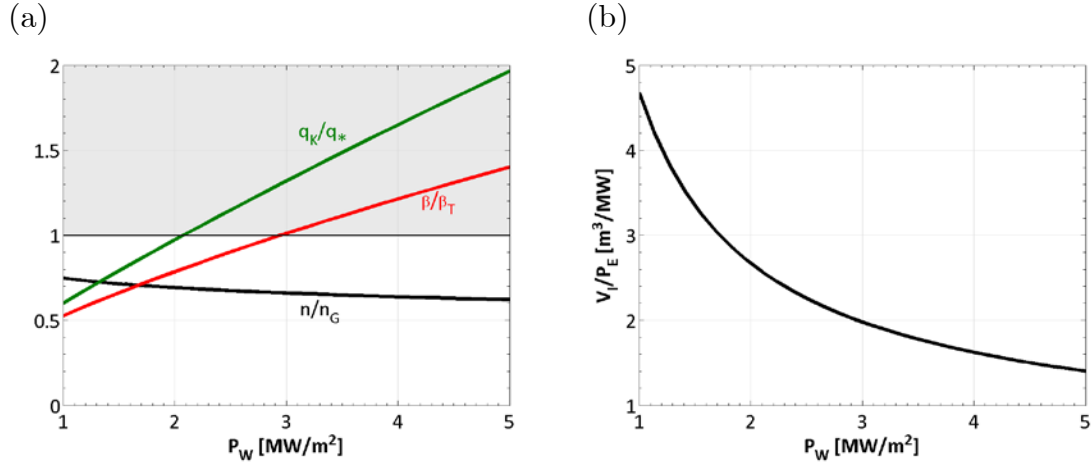
Figure 9 (a) Curves of $\bar{n}\,/\,n_G$, $b\,/\,b_T$, and $q_K\,/\,q_*$ as a function of $P_W$ for $H = 1$, $B_{\max} = 13\,T$, $P_E = 1000\,MW$ assuming that $f_B\,/\,f_{NC} = 1$. Successful operation corresponds to the unshaded region. (b) Corresponding curve of $V_I\,/\,P_E$ versus $P_W$.